J. Membrane Biol. 61, 173–192 (1981)

The Journal of
Membrane Biology

Phosphate Transport in Human Red Blood Cells: Concentration Dependence and pH Dependence of the Unidirectional Phosphate Flux at Equilibrium Conditions

K.F. Schnell, E. Besl and R. v. der Mosel

Institut für Physiologie, Universität Regensburg, Postfach 397, D-8400 Regensburg, Germany

Summary. The concentration dependence and the pH dependence of the phosphate transport across the red cell membrane were investigated. The unidirectional phosphate fluxes were determined by measuring the ^{32}P-phosphate self-exchange in amphotericin B (5 μmol/liter) treated erythrocytes at 25 °C.

The flux/concentration curves display an *S*-shaped increase at low phosphate concentrations, a concentration optimum in the range of 150 to 200 mM phosphate and a self-inhibition at high phosphate concentrations. The apparent half-saturation concentrations, $P_{(0.5)}$, range from 50 to 70 mM and are little affected by pH. The self-inhibition constants, as far as they can be estimated, range from 400 to 600 mM. The observed maximal phosphate fluxes exhibit a strong pH dependence. At pH 7.2, the actual maximal flux is 2.1×10^{-6} moles $\cdot$ min$^{-1} \cdot$ g cells^{-1}. The ascending branches of the flux/concentration curves were fitted to the Hill equation. The apparent Hill coefficients were always in the range of 1.5–2.0. The descending branches of the flux/concentration curves appear to follow the same pattern of concentration response.

The flux/pH curves were bell-shaped and symmetric with regard to their pH dependence. The pH optimum is at approximately pH 6.5–6.7. The apparent pK of the activator site is in the range of 7.0 to 7.2, while the apparent pK for the inactivating site is in the range of 6.2 to 6.5. The pK-values were not appreciably affected by the phosphate concentration.

According to our studies, the transport system possesses two transport sites and probably two modifier sites as indicated by the apparent Hill coefficients. In addition, the transport system has two proton binding sites, one with a higher pK that activates and one with a lower pK that inactivates the transport system. Since our experiments were executed under self-exchange conditions, they do not provide any information concerning the location of these sites at the membrane surfaces.

Key words: Erythrocyte membrane, phosphate transport, anion permeability, transport kinetics

The transport of chloride, bicarbonate, sulfate, and phosphate across the red cell membrane is mediated by a specific transport system termed the inorganic anion transport system. The inorganic anion transport system exhibits a saturation kinetics, a self-inhibition at high anion concentrations, a counter-acceleration, and a competition of various inorganic anions for the transport system [2, 7, 9–14, 17, 22–26, 28, 31, 36, 42, 54, 55, 58–60, 70, 73]. Moreover, the transport of the above anions can be inhibited by the same agents [8, 12, 13, 14, 19, 29, 33–35, 37, 43, 53]. Biochemical studies supply strong evidence for the assumption that the band-3-protein is involved in the transport of inorganic anions across the red cell membrane [3–6, 20, 21, 30, 38, 42, 44, 48, 49, 51, 52, 62, 63, 74, 77, 78]. Although great progress has been made concerning the elucidation of the structure and the function of the band-3-protein [16, 21, 45–47, 50, 64–69, 75, 76], the mechanism of the anion transport across the red cell membrane has not yet been resolved. Thus for the present, our knowledge of the mechanism of the anion transport is predominantly based upon a detailed analysis of the kinetics of the anion transport. For details, the reader is referred to the reviews of Deuticke [13], Cabantchik, Knauf and Rothstein [3] and of Knauf [28].

For the characterization of the inorganic anion transport system of the red cell membrane, the transport of a number of closely related anions has

0022-2631/81/0061-0173 $04.00

to be studied. This paper is concerned with the concentration dependence and the pH dependence of the unidirectional phosphate flux. The unidirectional phosphate flux exhibits an *S*-shaped concentration response at low phosphate concentrations, a flux optimum, and a self-inhibition at high phosphate concentrations. The flux/pH curves of phosphate are bell-shaped and closely resemble those of sulfate [7, 9–11, 18, 22–26, 42, 53–60, 73]. The kinetics of the phosphate transport points to a highly complex transport system for inorganic anions which consists of two transport sites, two modifier sites, and two proton binding sites. The transport sites and the modifier sites are involved in the binding of phosphate and account for the *S*-shaped concentration response and the self-inhibition of the phosphate flux. The proton binding sites regulate the activity of the transport system. Since the experiments were conducted under self-exchange conditions, no conclusive information is gained about the location of the different sites on the membrane surfaces.

Materials and Methods

Preparation of the red blood cells: Blood from healthy adult donors was used. The blood was withdrawn under sterile conditions and stored for 2–6 days at 4 °C. Coagulation was prevented by adding an acid-citrate-dextrose solution. Before beginning the experiments, the red blood cells were washed twice in a 165 mM KCl solution, whereby plasma and buffy coat were removed. 4 g tightly packed cells (centrifugation at 5,000 × *g* for 10 min at 20 °C, pH 7.2–7.3) were added to 36 ml of an isotonic K-phosphate solution (132 mM), pH 7.2, and incubated three times for 10 min at 37 °C. After depleting the cells of chloride, the cells were transferred into a K-phosphate/sucrose solution, pH 7.2, containing 75–400 mM K-phosphate, 30 mM sucrose, and 5 µmol/-liter amphotericin B. Sucrose does not penetrate the red cell membrane and was added in order to counterbalance the osmotic pressure of hemoglobin. Amphotericin B makes the red cell membrane leaky for potassium and permits a reduction of the intracellular salt concentration without the occurrence of hemolysis. In some experiments 10 µmol/liter valinomycin were added instead of amphotericin B. If required for the respective experiments, the phosphate concentrations then were titrated down to lower values by slowly adding a 30-mM sucrose solution. The lowest phosphate concentration used was 10 mM. The titration was performed with a 10% cell suspension and usually took 2 hr at 37°C, pH 7.2–7.3. After this period, an equilibrium distribution between intracellular and extracellular phosphate is reached. Trial runs with ^{32}P-phosphate labeled red cells were performed in order to test as to whether an equilibrium distribution of phosphate was reached.

After titration, the cells were spun down, the supernatant was removed, and the cells were then resuspended in a K-phosphate buffer/sucrose solution of appropriate composition (10–400 mM K-phosphate buffer, 30 mM sucrose, pH 6.2–8.6). No attempts were made to remove amphotericin B or valinomycin quantitatively from the cells. Each sample was subdivided into three portions. Portion 1 was labeled with ^{32}P-phosphate and employed for measuring the unidirectional phosphate flux. Portions 2 and 3 were used for determining the equilibrium distributions of phosphate and of chloride.

Preparation of red cell ghosts: The pH-response of the unidirectional phosphate flux was measured in amphotericin B treated red cells and red cell ghosts. The red cell ghosts were prepared according to the method of Bodemann and Passow [1] and of Lepke and Passow [32]. After resealing, the ghosts were titrated to the respective pH and labeled with either ^{32}P-phosphate plus D(1 – ^{3}H) glucose or ^{36}Cl-chloride plus D(1 – ^{3}H)glucose. The distributions of phosphate and of chloride, and the phosphate fluxes were measured in the same way as with intact red cells.

Determination of the Equilibrium Distribution of Phosphate and of Chloride

Technical procedure: The equilibrium distribution of phosphate and of chloride between intracellular and extracellular space was determined by using a double label technique, which permits the simultaneous counting of ^{32}P-phosphate and D(1 – ^{3}H)glucose or of ^{36}Cl-chloride and D(1 – ^{3}H)glucose. D(1 – ^{3}H)glucose was employed for monitoring the intracellular volume. The uptake of D(1 – ^{3}H)glucose is rapid and at 37 °C, an equilibrium distribution between intracellular and extracellular space is reached within 2 min. The metabolic degradation of D-glucose is slow, and the distribution of tritium between cells and extracellular solution remains stable for at least 30 min. At isotopic equilibrium the specific activities of phosphate, of chloride, and of D-glucose in the intracellular and in the extracellular solution are equal. The amount of inorganic phosphate, of chloride, and of D-glucose within the cells can be calculated from the ^{32}P-phosphate, ^{36}Cl-chloride, and D(1 – ^{3}H)glucose content of the cells and from the specific activities of the respective substances in the extracellular solution.

Aliquots of each sample were labeled with ^{32}P-phosphate and D(1 – ^{3}H)glucose, or with ^{36}Cl-chloride (1 mM Na[^{36}Cl]Cl) and D(1 – ^{3}H)glucose, respectively. Depending upon pH, the labeling of the cells with ^{32}P-phosphate took from 2–6 hr at 37 °C. 10–15 min before the end of the equilibration period, 10 mM of D(1 – ^{3}H)glucose were added. At the end of the labeling period, triplicate samples of 10 ml each were withdrawn and centrifuged for 10 min at 50,000 × g. The supernatant was removed. The cells were then lysed in 2 ml of distilled water by adding small amounts of saponin. The lysate and the supernatant were deproteinized by the addition of trichloracetic-acid. ^{32}P-phosphate, ^{36}Cl-chloride and D(1 – ^{3}H)glucose within the cell fraction and within the supernatant were counted. The phosphate concentration was measured photometrically. Chloride was determined by conductometric titration. The extracellular water trapped in the sediment amounts to approximately 2% of the total sediment volume. Therefore, no corrections for trapped extracellular radioactivity were made. The volume of the lysate fraction was checked by drying the lysate in the centrifuge tubes at 80 °C to constant weight.

The accuracy of the double label procedure was checked by separately measuring the ^{32}P-phosphate distribution, the ^{36}Cl-chloride distribution, and the D(1 – ^{3}H)glucose distribution. The ^{32}P-phosphate distribution and the ^{36}Cl-chloride distribution measured by the single label experiments were identical with those obtained from the double label experiments.

In order to test as to whether large amounts of ^{32}P-phosphate were incorporated into the organic phosphate pool, red cells were washed and incubated for 4 hr at 37 °C in a K-phosphate solution with high specific activity (20 mM K-phosphate, 120 mM KCl, and 30 mM sucrose). After incubation, the cells were washed, disintegrated, and the intracellular phosphates were separated by thin layer chromatography (TLC aluminium sheets, PEI-cellulose F precoated, Merck, Darmstadt, mobile phase: 0.1–1.0 M LiCl or 0.3 M Na_2CO_3). Although a number of organic phosphates

could be seen by inspection of the sheets under UV-light, the autoradiographs did not show a radioactive labeling of these compounds. The bulk radioactivity was found in the inorganic phosphate fraction. If small amounts of ^{32}P-phosphate were incorporated into the organic phosphate pool they, for our purposes, can be disregarded.

Calculations

The distribution ratios of inorganic phosphate, R_P, and of chloride, R_{Cl}, are defined by:

$$R_P = P_{(in)}/P_{(ex)} \tag{1}$$

$$R_{Cl} = Cl_{(in)}/Cl_{(ex)}. \tag{2}$$

At isotopic equilibrium, the specific activities in the extracellular and in the intracellular solutions are equal and the distribution of phosphate and of chloride can be computed as follows:

$$R_P = \frac{^{32}\text{P-CPM}_{(in)}/^{3}\text{H-CPM}_{(in)}}{^{32}\text{P-CPM}_{(ex)}/^{3}\text{H-CPM}_{(ex)}} \tag{3}$$

$$R_{Cl} = \frac{^{36}\text{Cl-CPM}_{(in)}/^{3}\text{H-CPM}_{(in)}}{^{36}\text{Cl-CPM}_{(ex)}/^{3}\text{H-CPM}_{(ex)}}. \tag{4}$$

In red cells the distribution of chloride and of protons follows a Donnan distribution, and the chloride distribution can be used for calculating the intracellular pH:

$$pH_{(in)} = pH_{(ex)} + \log R_{Cl}. \tag{5}$$

This relation is also valid under conditions where the equilibrium distribution of phosphate has not yet been attained. R_P reflects the distribution of the total inorganic phosphate between intracellular and extracellular space. Since the pK for the second dissociation step of *o*-phosphoric acid is 7.21 (25 °C) [71], inorganic phosphate under our experimental conditions is present as a monovalent $H_2PO_4^-$ and as a divalent HPO_4^{2-} anion. Thus, R_P and R_{Cl} cannot be directly compared. Knowing R_P and the intracellular pH, the distribution R_{P1} of $H_2PO_4^-$ is obtained by:

$$R_{P1} = \frac{H_{(in)}(K_P + H_{(ex)})}{H_{(ex)}(K_P + H_{(in)})} R_P \tag{6}$$

P – concentration of inorganic phosphate (M)
Cl – concentration of chloride (M)
H – concentration of protons (M)
^{32}P-CPM – radioactivity of phosphate (CPM/ml)
^{36}Cl-CPM – radioactivity of chloride (CPM/ml)
^{3}H-CPM – radioactivity of D(1 – ^{3}H)glucose (CPM/ml)
K_P – apparent dissociation constant of the second dissociation step of *o*-phosphoric acid (M).

The subscripts *in* and *ex* refer to the intracellular and to the extracellular space, respectively.

Determination of the Unidirectional Phosphate Flux

The unidirectional phosphate flux $\vec{J}_P$ was determined at Donnan equilibrium by measuring the ^{32}P-phosphate back-exchange from the radioactively labeled cells into a nonradioactive solution. The labeling of the cells was performed at 37 °C by using a 10% (wt/vol) cell suspension. The rate constant of the tracer back-exchange was measured with a 5% (wt/vol) cell suspension at 25 °C.

The unidirectional flux $\vec{J}_P$ is given by:

$$\vec{J}_P = k \cdot n_{in} \tag{7}$$

with k (min^{-1}) being the rate constant for the tracer efflux and n_{in} (moles/g cells) being the intracellular phosphate. n_{in} was computed from the radioactivity within the cell fraction at isotopic equilibrium and from the specific activity of phosphate in the extracellular solution. The rate constant k was determined by fitting the curves of ^{32}P-CPM *vs.* time to Eq. (8).

$$\ln(^{32}\text{P-CPM}_\infty - ^{32}\text{P-CPM}_t) = -k \cdot t + \ln(^{32}\text{P-CPM}_\infty - ^{32}\text{P-CPM}_0). \tag{8}$$

^{32}P-CPM$_0$, ^{32}P-CPM$_\infty$ and ^{32}P-CPM$_t$ are the radioactivities of phosphate in the extracellular solutions at zero time, infinite time, and at time t, respectively.

The fluxes were expressed in moles · min^{-1} · g cells^{-1}. The term "g cells" refers to the wet wt of tightly packed red blood cells under standardized conditions (centrifugation: 5,000 × *g* for 10 min at pH 7.2, 20 °C), and corresponds to 8×10^9 cells. (For details *see* [58]).

Plotting Procedures for the Flux/Concentration Curves

Transport equation: For the analysis of the *S*-shaped flux/concentration curves the Hill equation was used. Since the Hill equation cannot account for the self-inhibition at high anion concentration, the empirical term $K_{is}^n/(K_{is}^n + S^n)$ was introduced. in our notation, the extended Hill equation then reads:

$$\vec{J} = \vec{J}_{max(pH)} \frac{S^n \cdot K_{is}^n}{(K_s^n + S^n)(K_{is}^n + S^n)} \tag{9.1}$$

$\vec{J}$ – unidirectional flux
$\vec{J}_{max(pH)}$ – maximal unidirectional flux at constant pH
K_s, K_{is} – half-saturation constant and self-inhibition constant
n – Hill coefficient
S – anion concentration.

For S either the extracellular phosphate concentration, $P_{(ex)}$, the intracellular phosphate concentration, $P_{(in)}$, or the term $(P_{(in)} \cdot P_{(ex)})^{1/2}$ were inserted, depending upon whether the extracellular solution, the intracellular solution, or the middle of the membrane were chosen as a reference state [27]. For derivation of the Hill equation, *see* Segel, Enzyme Kinetics, pp. 360–377 [61]. The graphically determined values of K_s, $\vec{J}_{max(pH)}$, K_{is} and n were designated $K_{s(app)}$, $\vec{J}_{max(pH/app)}$, $K_{is(app)}$ and n_{app}.

The position of the concentration optimum: The slope of the flux/concentration curves is given by the first derivative $d\vec{J}/dS$ of Eq. (9.1). At the peak of the flux/concentration curves $d\vec{J}/dS = 0$ and we end up with the following relations [72]:

$$S_{opt}^2 = K_s \cdot K_{is} \tag{9.2}$$

and

$$\vec{J}_{max(opt/pH)} = \vec{J}_{max(pH)} \frac{S_{opt}^{2n}}{(K_s^n + S_{opt}^n)^2}. \tag{9.3}$$

S_{opt} is the anion concentration where the flux optimum is located, and $\vec{J}_{max(opt/pH)}$ the actual maximal flux at the concentration maximum of the flux/concentration curves. The other parameters have the same meanings as defined above. S_{opt} and $\vec{J}_{max(opt/pH)}$ can be directly taken from the flux/concentration curves. If the half-saturation constant K_s is known. then Eq. (9.2) can be used for estimating the self-inhibition constant K_{is}.

Table 1. Intercepts and slopes of the plotting procedures for the flux/concentration curves

	Plotting procedure		Slope	Intercepts	
	Ordinate	Abscissa		Ordinate	Abscissa
Ascending branch	$1/\vec{J}$	$1/S^n$	$K_s^n/\vec{J}_{max(pH)}$	$1/\vec{J}_{max(pH/app)}$	$-1/K_{s(app)}^n$
Ascending branch	$\vec{J}$	$\vec{J}/S^n$	$-K_{s(app)}^n$	$\vec{J}_{max(pH/app)}$	$\vec{J}_{max(pH)}/K_s^n$
Descending branch	$1/\vec{J}$	S^n	$1/(\vec{J}_{max(pH)} \cdot K_{is}^n)$	$1/\vec{J}_{max(pH/app)}$	$-K_{is(app)}^n$

$$K_{s(app)}^n = \frac{K_s^n \cdot K_{is}^n}{K_s^n + K_{is}^n}; \quad \vec{J}_{max(pH/app)} = \vec{J}_{max(pH)} \frac{K_{is}^n}{K_s^n + K_{is}^n}; \quad K_{is(app)} = K_s^n + K_{is}^n$$

Double logarithmic plot: The flux/concentration curves can be plotted in a double logarithmic form by plotting $\log J$ *vs.* $\log S$. For low S, Eq. (9.1) reduces to:

$$\log \vec{J} = \log(\vec{J}_{max(pH)}/K_s^n) + n \log S \tag{9.4.1}$$

while for high S Eq. (9.1) reduces to:

$$\log \vec{J} = \log(\vec{J}_{max(pH)} \cdot K_{is}^n) - n \log S. \tag{9.4.2}$$

At low S the plots of $\log \vec{J}$ *vs.* $\log S$ should yield straight lines with a slope of $+n$, while at high S the slope $-n$ should be attained. If the increasing branches of the flux/concentration curves and the decreasing branches follow the same pattern of concentrations response, then the plots of $\log J$ *vs.* $\log S$ should be symmetric.

If the self-inhibition is completely neglected, the Hill equation may be transformed to:

$$\log\left(\frac{\vec{J}}{\vec{J}_{max(pH)} - \vec{J}}\right) = n \log S + \log K_s^n. \tag{9.4.3}$$

Due to the self-inhibition $\vec{J}_{max(pH)}$ cannot be obtained directly from the flux/concentration curves and Eq. (9.4.3) in our case therefore cannot be used.

Plots: $1/\vec{J}$ *vs.* $1/S^n$; $\vec{J}$ *vs.* $\vec{J}/S^n$; $\vec{J}$ *vs.* S^n. From Eq. (9.1) a series of transformations can be made which should give linear plots for either the ascending or the descending branches of the flux/concentration curves. Multiplying the parenthetical term in the denominator of Eq. (9.1) and disregarding at low S the term S^{2n}, Eq. (9.1) may be written in its double reciprocal form:

$$\frac{1}{\vec{J}} = \frac{1}{\vec{J}_{max(pH)}}\left(\frac{K_s^n + K_{is}^n}{K_{is}^n} + \frac{K_s^n}{S^n}\right). \tag{9.5}$$

Alternatively, for low S, Eq. (9.1) may be rearranged to give:

$$\vec{J} = \vec{J}_{max(pH)} \frac{K_{is}^n}{K_s^n + K_{is}^n} - \frac{K_s^n \cdot K_{is}^n}{K_s^n + K_{is}^n}(\vec{J}/S^n). \tag{9.6}$$

Conversely, at high S, the term K_s^n in the denominator of Eq. (9.1) may become negligible and we end up with:

$$\frac{1}{\vec{J}} = \frac{1}{\vec{J}_{max(pH)}}\left(\frac{K_s^n + K_{is}^n}{K_{is}^n} + \frac{S^n}{K_{is}^n}\right). \tag{9.7}$$

According to Eqs. (9.5) and (9.6), linear plots can be constructed for the ascending branches of the flux/concentration curves by plotting $1/\vec{J}$ *vs.* S^n or by plotting $\vec{J}$ *vs.* $\vec{J}/S^n$. The apparent Hill coefficient n has to be varied until linearity is attained. The apparent maximal flux, $\vec{J}_{max(pH/app)}$, and the apparent half-saturation constants, $K_{s(app)}$, then are obtained from the intersections of the straight lines with the respective axes. In general, the self-inhibition is perceived in the plots by deviations from linearity. However, as far as the self-inhibition is linear it cannot be recognized from the graphs and the graphically determined values of $\vec{J}_{max(pH)}$ and K_s may be erroneously low. Theoretically, the concentration response of the descending branches of the flux/concentration curves can be examined in a similiar fashion by plotting $1/\vec{J}$ *vs.* S^n [Eq. (9.7)]. In our case, on the descending branches, a sufficient number of points was not available so that the pattern of concentration response could not be tested with the same accuracy as for the ascending branches of the flux/concentration curves. The intercepts and the slopes for the various plotting procedures are listed in Table 1.

Plotting Procedures for the Flux/pH Curves

Transport equation for a diprotic system: With respect to the phosphate transport, the inorganic anion transport system behaves as a diprotic system, which at high pH is activated and at low pH is inactivated by protons. As will be discussed later, the pH response of a diprotic system may be given by the following equation [Eq. (10.1)]:

$$\vec{J} = \vec{J}_{max(S)}/(1 + K_H/H + H/K_{iH}) \tag{10.1}$$

$\vec{J}$ – unidirectional flux
$\vec{J}_{max(S)}$ – maximal unidirectional flux at constant S
K_H, K_{iH} – dissociation constants of the activator and of the inhibitor site, respectively
H – proton concentration.

For H either the extracellular proton concentration, $H_{(ex)}$, or the intracellular proton concentration, $H_{(in)}$, were inserted, depending upon which side of the membrane was selected as a reference state. For details, *see* Segel, Enzyme Kinetics, pp. 884–924 [61].

Double logarithmic plot: The symmetry of the flux/pH curves can easily be tested by plotting $\log \vec{J}$ *vs.* pH. At high pH, when $H \ll K_H$, a limiting slope, $\Delta \log \vec{J}/\Delta \mathrm{pH}$, of -1 should be attained. Conversely, at low pH, when $H \gg K_{iH}$, the limiting slope should be equal to $+1$. If for technical reasons the above conditions for the limiting slopes cannot be fulfilled, a slope smaller than unity can be obtained, albeit deviations from linearity may already escape detection.

Plots: $1/\vec{J}$ *vs.* $1/H$; $\vec{J}$ *vs.* $\vec{J}/H$; $\vec{J}$ *vs.* H: Protons, as far as the upper branches of the flux/pH curves (pH > 6.5) are concerned, may be considered as an activator and, as far as the lower branches (pH < 6.5) are concerned, as an inhibitor of the transport system. For the determination of K_H and K_{iH} the upper and the lower branches of the flux/pH curves have to be examined separately. At high pH, the term H/K_{iH} can be ignored and Eq. (10.1) reduces to:

$$1/\vec{J} = (1 + K_H/H)/\vec{J}_{max(S)}. \tag{10.2}$$

Table 2. Intercepts and slopes of the plotting procedures of the flux/pH curves

	Plotting procedure		Slope	Intercepts	
	Ordinate	Abscissa		Ordinate	Abscissa
Right-hand side branch of the flux/pH curve	$1/\vec{J}$	$1/H$	$K_H/\vec{J}_{max(S)}$	$1/\vec{J}_{max(S)}$	$-1/K_H$
Right-hand side branch of the flux/pH curve	$\vec{J}$	$\vec{J}/H$	$-K_H$	$\vec{J}_{max(S)}$	$\vec{J}_{max(S)}/K_H$
Left-hand side branch of the flux/pH curve	$1/\vec{J}$	H	$1/(J_{max(S)} \cdot K_{iH})$	$1/\vec{J}_{max(S)}$	$-K_{iH}$

Alternatively, disregarding the term H/K_{iH}, Eq. (10.1) can be rearranged as follows:

$$\vec{J} = \vec{J}_{max(S)} - K_H(\vec{J}/H). \tag{10.3}$$

On the other hand, at low pH, the term K_H/H can be ignored and Eq. (10.1) then may be rewritten as:

$$1/\vec{J} = (1 + H/K_{iH})/\vec{J}_{max(S)}. \tag{10.4}$$

The apparent values of $\vec{J}_{max(S)}$, K_H and K_{iH} were obtained from the slopes and the intercepts of the axes as listed in Table 2.

Determination of the pK-values from the pH optimum and the pH values at half-maximal flux: If K_H and K_{iH} are less than 2 pH units apart, and if the flux/pH curve is symmetric, then the dissociation constants can be calculated from the position at the pH optimum and the pH values where the half-maximal flux is attained. At the peak of the flux/pH curves, the first derivative $d\vec{J}/dH$ of Eq. (10.1) is equal to zero and we obtain:

$$H^2_{opt} = K_H \cdot K_{iH}. \tag{10.5}$$

Furthermore, the pH optimum, pH_{opt}, and the pH values $pH_{(H/0.5)}$ and $pH_{(iH/0.5)}$, at both sides of the pH optimum, where one-half of the maximal flux is attained may be read from the flux/pH curves as shown in Fig. 9. According to Segel the following expression can be derived:

$$H_{(H/0.5)} + H_{(iH/0.5)} = K_{iH} + 4H_{opt}. \tag{10.6}$$

Using Eqs. (10.5) and (10.6), the pH optimum and the pH values at one-half maximal flux can be employed for the calculation of the respective pK-values. (For details, *see* Segel, pp. 914–917 [61] and Webb, pp. 660–661 [72].)

Chemicals

All chemicals employed were of AR grade. Amphotericin B was kindly supplied by v. Heyden-Squibb (Regensburg); valinomycin was purchased from Boehringer GmbH, Mannheim. For the phosphate determination, Merckotest inorganic phosphate (No. 3311) was used. ^{36}Cl-chloride and ^{32}P-orthophosphate were obtained from Amersham Buchler.

Results

Concentration Dependence of the Unidirectional Phosphate Flux

The equilibrium distributions of *o*-phosphate and of chloride between intracellular and extracellular space were determined as a function of the extracellular pH and of the extracellular phosphate concentration as indicated in the methods section. From these values, the intracellular pH, the intracellular phosphate concentration, and the distribution of monovalent phosphate anions were calculated by using Eqs. (3)–(6). The results are listed in Table 3. Since the chloride self-exchange is two to three orders of magnitudes faster than the phosphate self-exchange, the chloride anions may be used for monitoring the actual membrane potential.

The equilibrium distribution of the total *o*-phosphate, R_p, and of chloride, R_{Cl}, were strongly affected by the extracellular pH and the extracellular phosphate concentration. At low pH and at low extracellular phosphate concentrations, the intracellular concentrations of phosphate and of chloride are greater than the extracellular concentrations and the respective distribution ratios, R_p and R_{Cl}, are greater than unity. At high pH, the intracellular phosphate concentrations and the intracellular chloride concentrations were smaller than the extracellular concentrations, and accordingly the distribution ratios, R_p and R_{Cl}, are smaller than unity. A more close inspection of Table 3 reveals differences between R_p and R_{Cl}. Since under ideal conditions the distribution of anions should follow a Donnan distribution, these differences are to be expected. Within the pH range of 6.0 to 8.6, which is of particular interest for our experiments, *o*-phosphate is present as monovalent $H_2PO_4^-$ and as divalent HPO_4^{2-} anion. R_p as calculated from the distribution of ^{32}P-phosphate at isotopic equilibrium reflects the distribution of the total *o*-phosphate. If R_{Cl} is greater than unity, R_p should be greater than R_{Cl}. On the other hand, if R_{Cl} is smaller than unity, R_p should be smaller than R_{Cl}. In order to test as to whether a true equilibrium distribution of *o*-phosphate was reached, the distribution of monovalent phosphate, R_{P1}, between intracellular and extracellular space was calculated. The comparison of R_{P1} and R_{Cl} shows that under most conditions R_{P1} is equal to R_{Cl}. This indicates that under most conditions a true equilibrium distribution of *o*-phosphate was reached. At pH 8.6 and at an extracellular phosphate concentration of greater than 100 mM, however, R_{Cl} is much greater than R_{P1}, indicating that under these conditions the uptake of ^{32}P-phos-

Table 3. Equilibrium distribution of phosphate and chloride as a function of the extracellular pH and the extracellular phosphate concentration

$pH_{(ex)}$	$P_{(ex)}$	R_P	R_{Cl}	$pH_{(in)}$	$P_{(in)}$	R_{P1}
6.3	25	1.65±0.08	1.49±0.05	6.47	41.25	1.51
	50	1.51±0.08	1.40±0.06	6.45	75.50	1.41
	75	1.39±0.04	1.30±0.03	6.41	104.25	1.32
	100	1.31±0.06	1.21±0.08	6.38	131.00	1.26
	150	1.21±0.03	1.15±0.05	6.36	181.50	1.18
	200	1.12±0.03	1.13±0.04	6.35	224.00	1.09
	250	1.05±0.04	1.10±0.05	6.34	262.50	1.03
	300	1.04±0.04	1.07±0.03	6.33	312.00	1.03
	400	0.98±0.06	1.05±0.05	6.32	392.00	0.97
6.5	30	1.52±0.06	1.38±0.05	6.64	45.60	1.38
	60	1.36±0.08	1.24±0.07	6.59	81.60	1.28
	100	1.26±0.09	1.15±0.05	6.56	126.00	1.21
	150	1.17±0.07	1.11±0.05	6.55	175.50	1.14
	200	1.08±0.03	1.11±0.06	6.55	216.60	1.05
	250	1.05±0.04	1.07±0.05	6.53	262.50	1.03
	300	0.98±0.06	1.06±0.07	6.53	294.00	0.96
	400	0.91±0.03	1.07±0.03	6.53	364.00	0.89
7.2	10	1.36±0.06	1.12±0.12	7.27	13.60	1.22
	25	1.11±0.06	1.03±0.07	7.21	27.75	1.09
	50	0.98±0.09	0.92±0.05	7.16	49.00	1.03
	75	0.89±0.06	0.89±0.03	7.15	66.75	0.96
	100	0.84±0.04	0.87±0.08	7.14	84.00	0.92
	150	0.78±0.03	0.84±0.07	7.12	117.00	0.87
	200	0.78±0.05	0.82±0.07	7.11	156.00	0.88
	300	0.70±0.03	0.84±0.08	7.13	240.00	0.77
	400	0.64±0.03	0.82±0.09	7.11	256.00	0.72
7.4*	25	1.03±0.04	1.00±0.05	7.40	26.80	1.03
	50	0.92±0.06	0.93±0.04	7.37	46.00	0.97
	75	0.85±0.05	0.89±0.05	7.35	64.00	0.93
	100	0.82±0.03	0.87±0.05	7.34	82.00	0.91
	150	0.76±0.07	0.84±0.04	7.32	114.00	0.86
	200	0.76±0.03	0.83±0.07	7.32	152.00	0.87
	300	0.70±0.05	0.85±0.05	7.33	210.00	0.79
	400	0.66±0.04	0.81±0.03	7.31	264.00	0.77
7.8	25	0.87±0.03	0.93±0.05	7.77	21.75	0.93
	50	0.79±0.02	0.89±0.03	7.75	39.50	0.87
	75	0.76±0.04	0.87±0.04	7.74	57.00	0.86
	100	0.78±0.03	0.90±0.05	7.75	78.00	0.85
	150	0.72±0.03	0.86±0.06	7.72	108.00	0.84
	200	0.72±0.05	0.84±0.03	7.72	144.00	0.84
	300	0.69±0.05	0.86±0.02	7.73	207.00	0.79
	400	0.64±0.03	0.88±0.05	7.74	256.00	0.72
8.6	30	0.72±0.03	0.78±0.03	8.49	21.60	0.92
	60	0.69±0.04	0.88±0.04	8.55	41.40	0.77
	100	0.68±0.03	0.88±0.05	8.54	68.00	0.77
	150	0.67±0.03	0.91±0.06	8.56	100.50	0.73
	200	0.65±0.02	0.94±0.08	8.57	130.00	0.69
	300	0.63±0.01	1.00±0.10	8.60	192.00	0.64
	400	0.60±0.02	1.07±0.09	8.63	240.00	0.56

$pH_{(ex)}$, $pH_{(in)}$ = extracellular and intracellular pH;
$P_{(ex)}$, $P_{(in)}$ = extracellular and intracellular concentrations of *o*-phosphate (mM);
$P_{1(ex)}$, $P_{1(in)}$ = extracellular and intracellular concentrations of $H_2PO_4^-$ (mM);
$R_P = P_{(in)}/P_{(ex)}$; $R_{Cl} = Cl_{(in)}/Cl_{(ex)}$; $R_{P1} = P_{1(in)}/P_{1(ex)}$.
The experiments were conducted with amphotericin B (5 μmol/liter) treated red cells, the experiments marked by * were performed with valinomycin (10 μmol/liter) treated red cells. The red cells were incubated in a solution containing *x* mM K-phosphate, 1 mM NaCl and 30 mM sucrose at different pH. Cell concentration 10% (wt/vol). Temperature, 37 °C. Incubation period, 4–6 hr. The phosphate distribution R_P, the chloride distribution R_{Cl} and the distribution of monovalent phosphate R_{P1} were determined by a double label technique using either ^{32}P-phosphate and D(1−^{3}H)-glucose or ^{36}Cl-chloride and D(1−^{3}H)-glucose as tracers. The intracellular phosphate concentrations $P_{(in)}$ and the intracellular $pH_{(in)}$ were calculated according Eqs. (5) and (6). For details, *see* the methods section.

phate by the red cells is too slow to reach an equilibrium distribution.

The intracellular pH was calculated from the extracellular pH and the chloride distribution R_{Cl}. The calculation of the intracellular pH is based upon the assumption that the distribution of protons between intracellular and extracellular space also follows a Donnan distribution. If the extracellular pH is adjusted to a distinct value and if the Donnan distribution of anions changes, then the intracellular pH cannot be kept constant. However, as can be seen from Table 3, the variations of the intracellular pH are small and amount maximally to 0.2 pH units.

The concentration response of the unidirectional phosphate flux at different pH is shown in Figs. 1 and 2. The unidirectional phosphate fluxes were plotted either *vs.* the extracellular or *vs.* the intracellular phosphate concentrations. The fluxes were all plotted on the same scale. For technical reasons the experiments were executed with amphotericin B (5 μmol/liter) or valinomycin (10 μmol/liter) treated red cells. Amphotericin B and valinomycin at low concentrations have no effect upon the unidirectional phosphate flux under self-exchange conditions [15]. At low phosphate concentrations, the flux/concentration curves exhibit an *S*-shaped increase of the flux. The phosphate fluxes then pass through a concentration maximum, while at high phosphate concentrations a self-inhibition of the phosphate fluxes is observed.

For characterizing the flux/concentration curves, the half-saturation concentrations, $P_{(0.5)}$, the location of the flux optimum, $P_{(opt)}$, and the actual maximal phosphate flux at constant pH, $\vec{J}_{max(opt/pH)}$, may be taken directly from the flux/concentration curves. The values obtained with reference to the extracellular (index ex) and with reference to the intracellular phosphate concentrations (index in) are listed in Tables 4 and 5. The half-saturation concentrations, $P_{(0.5/ex)}$ and $P_{(0.5/in)}$, range from 50–75 mM. $P_{(0.5/ex)}$ increases slightly with increasing pH, while $P_{(0.5/in)}$ shows a reverse pH response. $P_{(opt/ex)}$ and $P_{(opt/in)}$ are in the range of 140 to 200 mM. In

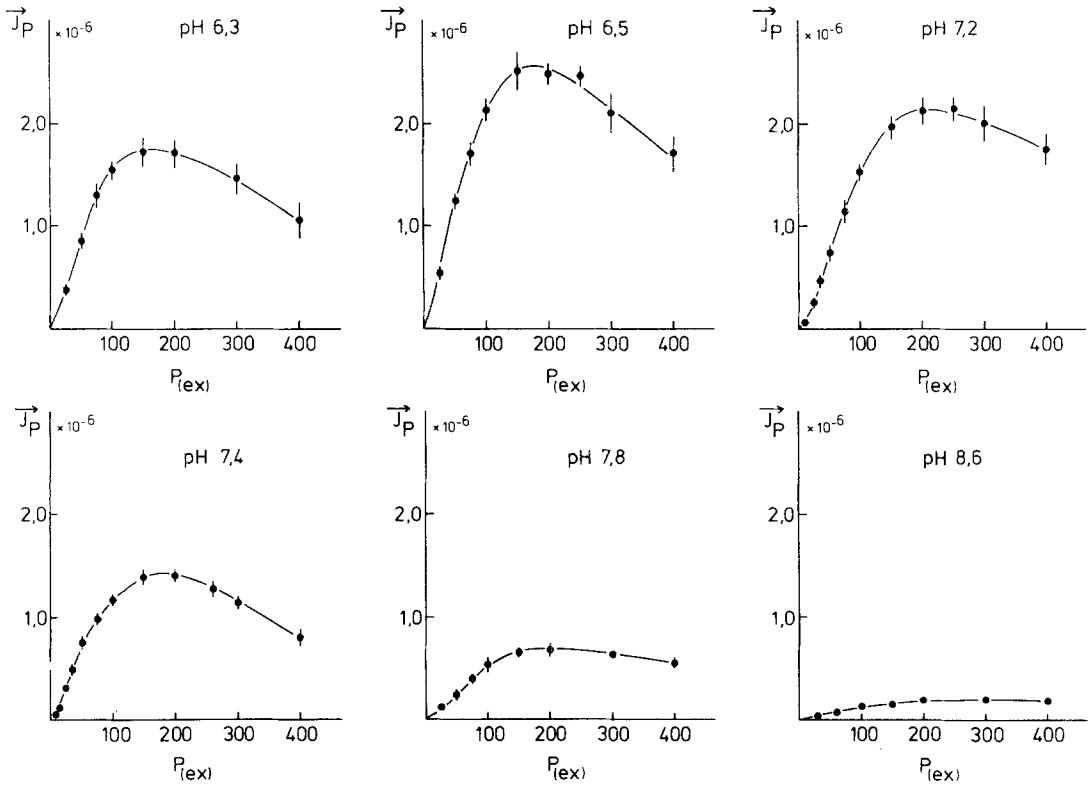

Fig. 1. Concentration dependence of the unidirectional phosphate flux as a function of the extracellular phosphate concentration. The experiments were performed with amphothericin B (5 μmol/liter) treated red cells, the experiments at pH 7.4 with valinomycin (10 μmol/-liter) treated red cells. The ^{32}P-phosphate back-exchange of a 5% (wt/vol) cell suspension was measured under self-exchange conditions at 25 °C. The unidirectional fluxes were calculated according to Eqs. (7) and (8). (For details *see* methods section.) Each point represents the mean of 3–4 experiments, the vertical bars denote the standard deviation. The extracellular pH is indicated in the figures. *Ordinate:* Unidirectional phosphate flux, $\vec{J}_P$, [moles/(min · g cells)]; *abscissa:* Extracellular phosphate concentration, $P_{(ex)}$ (mM)

contrast to $P_{(0.5/ex)}$ and $P_{(0.5/in)}$, $\vec{J}_{max(opt/pH)}$ displays a strong pH dependency. The pH-maximum of the flux is located at about pH 6.5. At pH 7.2, the actual maximal flux, $\vec{J}_{max(opt/pH)}$, is equal to $2.1 \cdot 10^{-6}$ moles/(min · g cells). A crude estimate of the self-inhibition constants can be made from the position of the flux-optimum by using Eq. (9.2) and inserting $P_{(0.5)}$ as an approximation for K_s. The self-inhibition constants as obtained by this procedure are in the range of 400–700 mM.

For a more detailed analysis of the flux/concentration curves, plotting procedures were used which are common in enzyme kinetics. Figure 3 exhibits the Lineweaver-Burk and the Woolf-Augustison-Hofstee plots of the flux/concentration curves at pH 7.2 with reference to the extracellular phosphate concentration, $P_{(ex)}$, and with reference to the intracellular phosphate concentration $P_{(in)}$. Similiar plots were obtained for the flux/concentration curves, measured at other pH values. It is obvious that the plots do not fit the experimental data. Both the Lineweaver-Burk and the Woolf-Augustison-Hofstee plots display curved lines for the ascending branches of the flux/concentration curves which confirm that the flux/concentration curves do not follow a simple Michaelis-Menten kinetics. Attempts to determine the apparent half-saturation constant $K_{s(app)}$ and the apparent maximal flux $\vec{J}_{max(pH/app)}$ by extrapolating from the fluxes measured at low phosphate concentrations, in both cases yielded negative values for $K_{s(app)}$ and for $\vec{J}_{max(pH/app)}$. Likewise, the Dixon plots made from the descending branches of the flux/concentration curves did not show straight lines.

In Figs. 4 and 5, the double reciprocal Hill plots and the Woolf-Augustison-Hofstee form of the Hill plot are shown. The curves were fitted with reference to the term $(P_{(ex)} \cdot P_{(in)})^{n/2}$ by varying n until linear plots for the ascending branches of the flux/concentration curves were obtained. For the double reciprocal plots, only the ascending branches of the flux/concentration curves were used. The parameters obtained from the curve-fitting procedure are listed in Table 6. The apparent Hill coefficients n_{app} were always within the range of 1.6–1.8. The apparent half-saturation constants, $K_{s(app)}$, amounted to approximately 80 mM and were little affected by pH. In

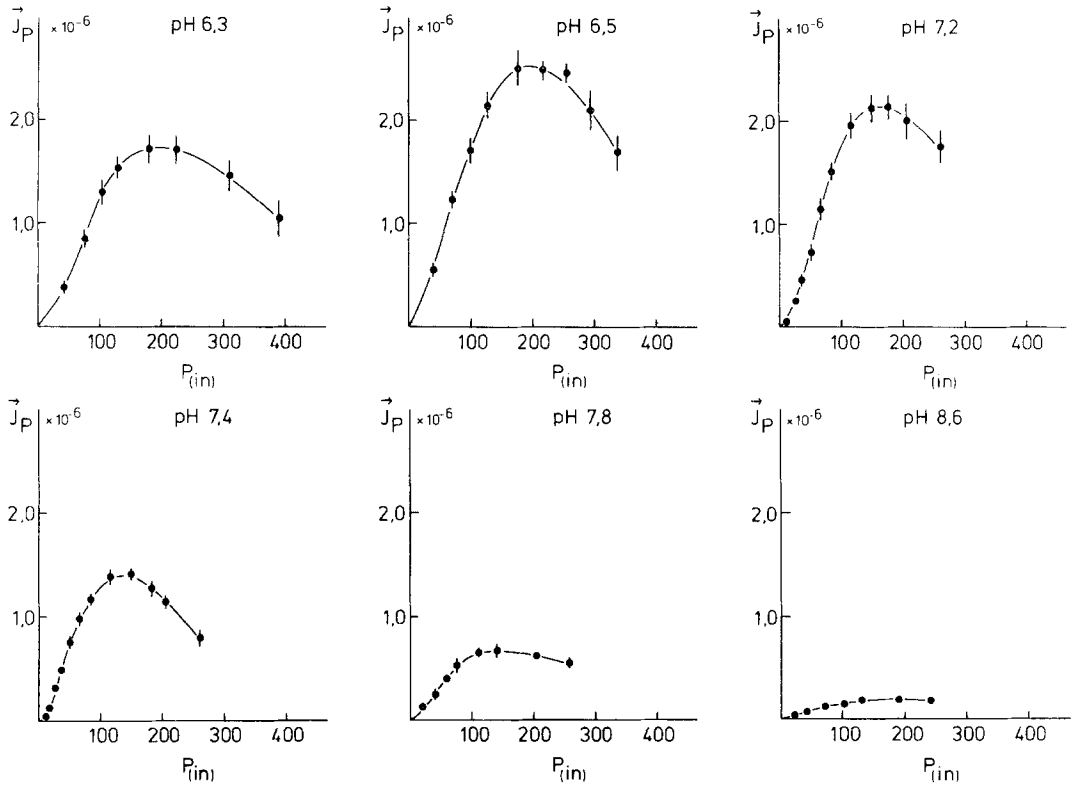

Fig. 2. Concentration dependence of the unidirectional phosphate flux as a function of the intracellular phosphate concentration. The same experiments as shown in Fig. 1 were used. The unidirectional phosphate flux is plotted *vs.* the intracellular phosphate concentration. For the identification of the flux/concentration curves, the extracellular pH is indicated in the figures. The intracellular pH may be taken from Table 3. *Ordinate:* Unidirectional phosphate flux, $\vec{J}_P$ (moles/(min · g cells)); *Abscissa:* Intracellular phosphate concentration, $P_{(in)}$ (mM)

Table 4. Analysis of the flux/concentration curves with respect to the extracellular phosphate concentration[a]

$pH_{(ex)}$	$P_{(0.5/ex)}$ (mM)	$P_{(opt/ex)}$ (mM)	$\vec{J}_{max(opt/pH)}$ [moles/(min · g cells)]	$K_{is(ex)}$ (mM)
6.3	53	150	1.72×10^{-6}	420
6.5	53	180	2.56×10^{-6}	610
7.2	68	200	2.12×10^{-6}	580
7.4*	55	180	1.42×10^{-6}	590
7.8	67	200	6.80×10^{-7}	597
8.6	70	(250)	1.95×10^{-7}	(892)

[a] The phosphate half-saturation concentrations $P_{(0.5/ex)}$, the position of the flux optimum, $P_{(opt/ex)}$, and the observed maximal unidirectional phosphate flux $J_{max(opt/pH)}$ were directly taken from the flux/concentration curves shown in Fig. 1. In the last column an estimate of the self-inhibition constant $K_{is(ex)}$ is given (*cf.* text). At pH 8.6, $P_{(opt/ex)}$ is difficult to determine. Therefore, the values for $P_{(opt/ex)}$ and for $K_{is(ex)}$ were put in parentheses. The experiments were conducted with amphotericin B(5 µmol/liter) treated cells; the experiment marked by * was performed with valinomycin (10 µmol/liter) treated cells.

Table 5. Analysis of the flux/concentration curves with respect to the intracellular phosphate concentration[a]

$pH_{(ex)}$	$pH_{(in)}$	$P_{(0.5/in)}$ (mM)	$P_{(opt/in)}$ (mM)	$\vec{J}_{max(opt/pH)}$ [moles/(min · g cells)]	$K_{is(in)}$ (mM)
6.3	6.47–6.32	75	180	1.72×10^{-6}	420
6.5	6.64–6.53	73	180	2.56×10^{-6}	440
7.2	7.27–7.11	63	160	2.12×10^{-6}	410
7.4[b]	7.40–7.31	51	150	1.42×10^{-6}	440
7.8	7.77–7.31	50	140	6.80×10^{-7}	390
8.6	8.49–8.63	56	(160)	1.95×10^{-7}	(460)

[a] The phosphate half-saturation concentrations $P_{(0.5/in)}$ with regard to the intracellular phosphate concentration (index in), the position of the concentration optimum $P_{(opt/in)}$ and the observed maximal unidirectional phosphate flux $J_{max(opt/pH)}$ were directly taken from the flux/concentration curves shown in Fig. 2. The self-inhibition constant $K_{is(in)}$ was calculated from the position of the flux-optimum as described in the text. In the second column, the range of the intracellular pH_{in} is tabulated. The flux optimum at pH 8.6 cannot be precisely determined. Therefore the values for $P_{(opt/in)}$ and $K_{is(in)}$ were put in parentheses.

[b] The experiments at pH 7.4 were executed with 10 µmol/liter valinomycin. The other experiments were executed with 5 µmol/liter amphotericin B.

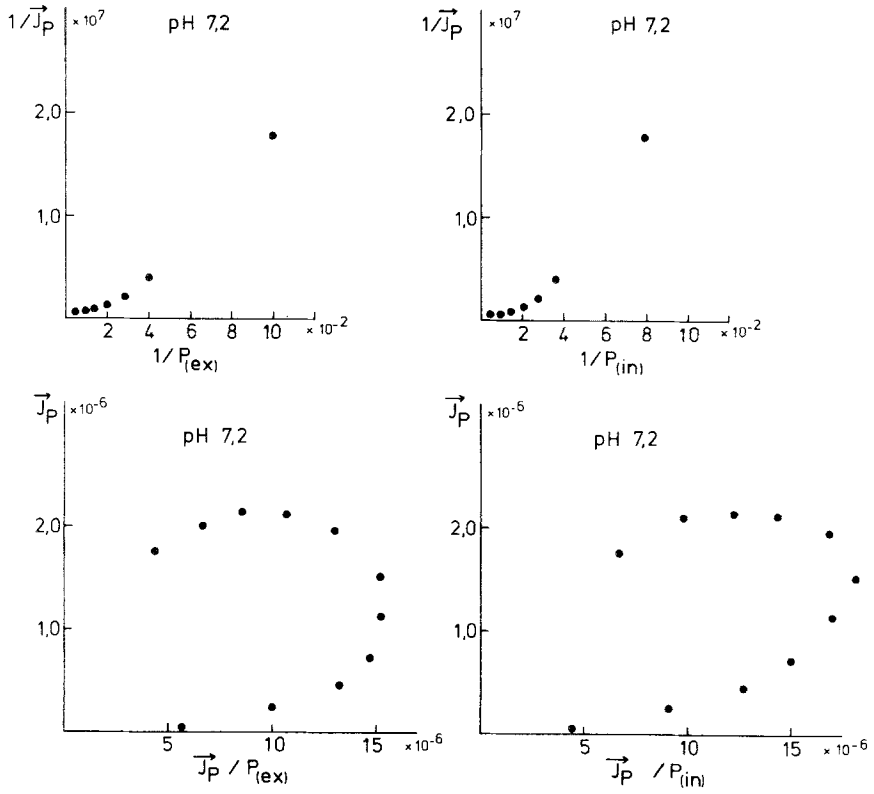

Fig. 3. Lineweaver-Burk and Woolf-Augustison-Hofstee plots of the flux/concentration curves. The Lineweaver-Burk and the Woolf-Augustison-Hofstee plots of the flux/concentration curves at pH 7.2 (Figs. 1 and 2) are shown. The plots were made with reference to the extracellular phosphate concentration, $P_{(ex)}$, and with reference to the intracellular phosphate concentration, $P_{(in)}$, respectively. Lineweaver-Burk plots (upper two curves): *Ordinate:* $1/\vec{J}_P$ (moles/(min · g cells))$^{-1}$, *abscissa:* $1/P_{(ex)}$ and $1/P_{(in)}$ (mM)$^{-1}$. Only the points from the ascending branches of the flux/concentration curves were employed. Woolf-Augustison-Hofstee plots (lower two curves): *Ordinate:* $\vec{J}_P$ (moles/(min · g cells)), *abscissa:* $\vec{J}_P/P_{(ex)}$ and $\vec{J}_P/P_{(in)}$ ((moles · min^{-1} · g cells^{-1})/M). All points of the respective flux/concentration curves are shown

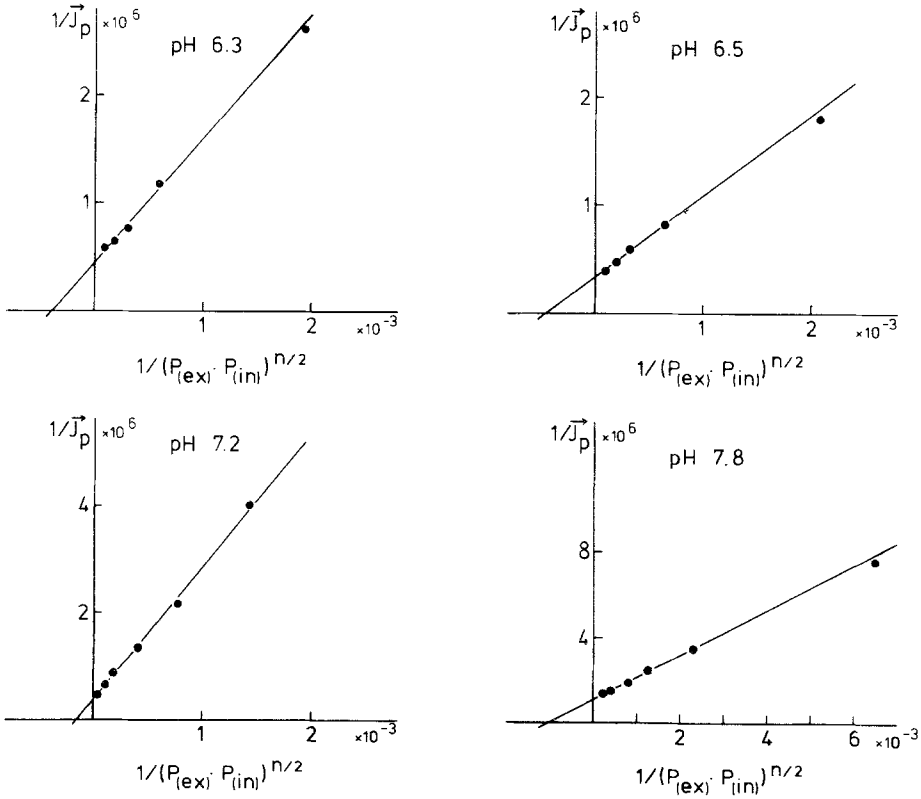

Fig. 4. Double reciprocal Hill plot with reference to the term $(P_{(ex)} \cdot P_{(in)})^{n/2}$. The Hill plots were made from the ascending branches of the flux/concentration curves as shown in Figs. 1 and 2. The linear graphs were constructed by variation of n until a linear relation between $1/\vec{J}_P$ and $1/(P_{(ex)} \cdot P_{(in)})^{n/2}$ was obtained. The parameters obtained from the plots are listed in Table 6. *Ordinate:* $1/\vec{J}_P$ (moles/(min · g cells))$^{-1}$; *Abscissa:* $1/(P_{(ex)} \cdot P_{(in)})^{n/2}$ [(mM)$^{-n/2}$]

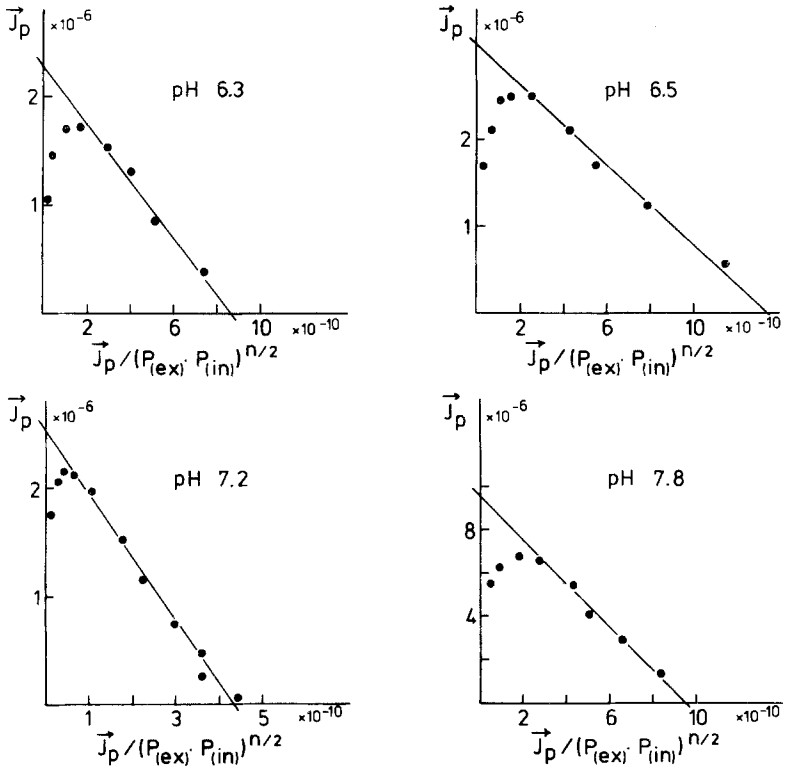

Fig. 5. Plot of $\vec{J}_P$ *vs.* $\vec{J}_P/P_{(ex)} \cdot P_{(in)})^{n/2}$. For the ascending branches of the flux/concentration curves a linear relation between $\vec{J}_P$ and $\vec{J}_P/(P_{(ex)} \cdot P_{(in)})^{n/2}$ is attained by varying n. The linearity for the ascending branches are indicated by the straight lines. The points positioned on the descending branches of the flux/concentration curves fall below the straight lines and were not used for the curve fitting procedure

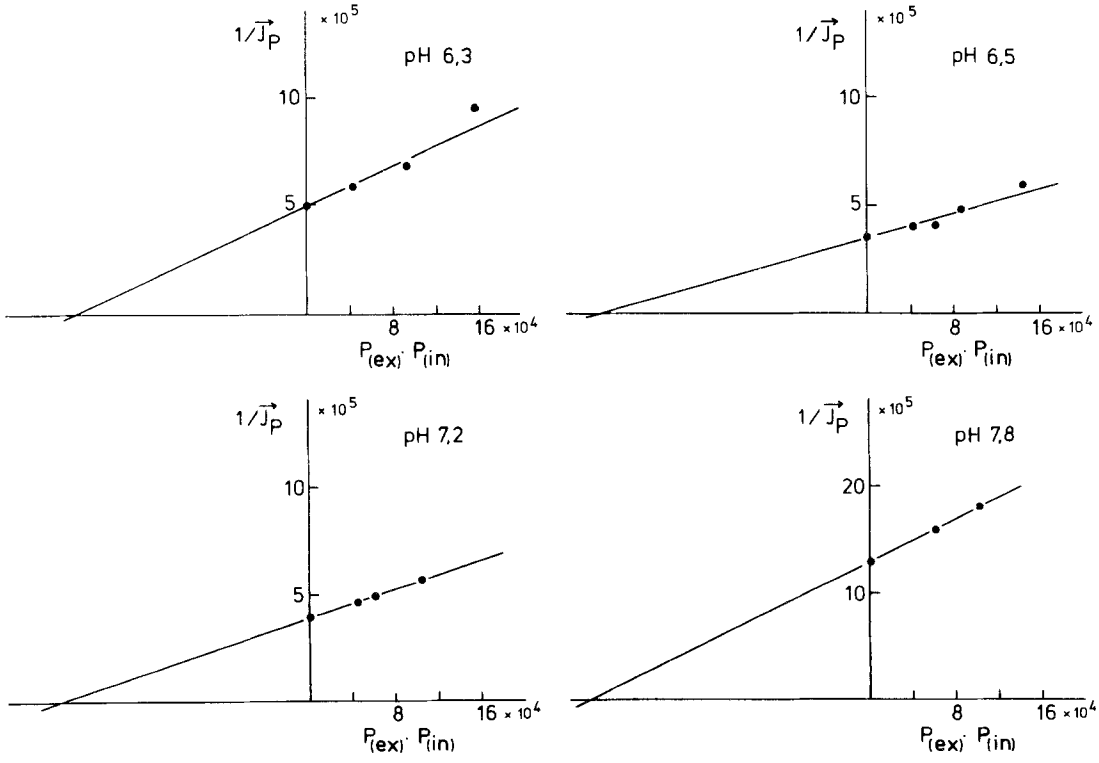

Fig. 6. Plot of $1/\vec{J}_P$ *vs.* $(P_{(ex)} \cdot P_{(in)})^{n/2}$. The descending branches of the flux/concentration curves were used for the plots. The reciprocal phosphate flux $1/\vec{J}_P$ (moles/(min · g cells))$^{-1}$ was plotted *vs.* $(P_{(ex)} \cdot P_{(in)})^{n/2}$ $(mM)^{n/2}$ by setting n equal to 2. The intersection points of the straight lines with the $1/\vec{J}_P$-axis from the corresponding double reciprocal plots were inserted as an additional point

Table 6. Hill plot parameters[a]

$pH_{(ex)}$	n_{app}	$K_{s(app)}$(mM)	$\vec{J}_{max(pH/app)}$[moles/(min · g cells)]
6.3	1.6–1.8	85.4±7.9	$2.51\pm0.37\times10^{-6}$
6.5	1.6–1.8	80.1±8.7	$3.33\pm0.27\times10^{-6}$
7.2	1.6–1.8	79.5±9.0	$3.05\pm0.36\times10^{-6}$
7.4	1.6–1.8	73.7±8.1	$2.10\pm0.24\times10^{-6}$
7.8	1.6–1.8	72.3±5.9	$9.28\pm0.78\times10^{-7}$
8.6	1.6–1.8	78.3±7.4	$2.19\pm0.20\times10^{-7}$

[a] The parameters were obtained from Hill plots as shown in Figs. 4 and 5. Mean value ± standard deviation of 3–4 experiments are listed in the table. The experiments were separately analyzed and thereafter the mean was calculated. The flux/concentration curves were fitted with reference to the term $(P_{(ex)}\cdot P_{(in)}{}^{n/2}$. The concentration optimum of the curves is positioned at 171±9 mM. The apparent self-inhibition constant, $K_{is(app)}$, was estimated by using Eq. (9.2). $K_{is(app)}=375\pm56$ mM. n_{app}=apparent Hill coefficient, $K_{s(app)}$=apparent half-saturation constant, and $\vec{J}_{max(pH/app)}$=apparent maximal flux at constant pH.

Table 7. Equilibrium distribution of phosphate R_P and of chloride R_{Cl} in red cells and red cell ghosts[a]

$pH_{(ex)}$	R_P	R_{Cl}	$pH_{(in)}$	R_{P1}
Amphotericin B-treated red blood cells (25 °C)				
5.5	1.62±0.09	1.60±0.10	5.70	1.59
6.0	1.36±0.06	1.33±0.07	6.12	1.32
6.5	1.10±0.05	1.08±0.05	6.53	1.08
7.0	0.89±0.04	0.91±0.06	6.96	0.93
7.5	0.72±0.05	0.81±0.06	7.41	0.84
8.0	0.64±0.06	0.80±0.03	7.90	0.78
8.5	0.62±0.04	0.83±0.04	8.42	0.74
9.0	0.61±0.03	0.89±0.04	8.95	0.69
Red cell ghosts (25 °C)				
6.0	1.18±0.05	1.15±0.03	6.06	1.16
6.3	1.22±0.03	1.14±0.04	6.36	1.19
6.5	1.20±0.07	1.17±0.03	6.57	1.15
6.8	1.17±0.05	1.14±0.06	6.86	1.11
7.0	1.20±0.04	1.12±0.05	7.05	1.13
7.2	1.19±0.06	1.12±0.06	7.25	1.11
7.5	1.18±0.05	1.09±0.04	7.54	1.10
8.0	1.16±0.02	1.08±0.03	8.03	1.08

[a] Amphotericin B (5 μmol/liter) treated red cells or red cells ghosts were incubated for 4 hr (37 °C) in a K-phosphate/NaCl sucrose solution (130 mM K-phosphate, 1 mM NaCl, 30 mM sucrose) at various pH. The solutions were labeled either with ^{32}P-phosphate or with ^{36}Cl-chloride. 10 mM D $(1-{}^3H)$-glucose were added 15 min before the end of the incubation period. The phosphate distribution $R_P=P_{(in)}/P_{(ex)}$, the chloride distribution $R_{Cl}=Cl_{in}/Cl_{(ex)}$, the intracellular pH_{in} and the distribution of $H_2PO_4^-$, R_{P1}, were determined by the use of a double-label technique as described in the methods section. The experiments were performed with a 10% (wt/vol) cell suspension or with a ghost suspension containing the same number of ghosts per volume.

contrast, the apparent maximal phosphate fluxes $\vec{J}_{max(pH/app)}$ exhibit a pronounced pH-dependence. Fits of the same quality were obtained when the flux/concentration curves were assessed with reference to the extracellular phosphate concentrations or with reference to the intracellular phosphate concentrations. The apparent Hill coefficients were always within the range of 1.5–2.0, but the intercepts on the axes were slightly different.

The concentration response pattern of the self-inhibition is difficult to examine. In most cases, we run into difficulties because only a few points were available on the descending branches of the flux/-concentration curves. Theoretically, the concentration response can be tested by using double logarithmic plots. If the self-inhibition follows the same pattern of concentration response as the initial increase of the flux at low anion concentrations, then the curves should be symmetric. The plots of $\log\vec{J}_P$ *vs.* $\log P_{(ex)}$ and of $\log\vec{J}_P$ *vs.* $\log P_{(in)}$ exhibited a slight asymmetry, while the plots of $\log\vec{J}_P$ *vs.* $\log(P_{(ex)}\cdot P_{(in)})^{1/2}$ seemed to be symmetric. As an additional test, the inverse phosphate flux $1/\vec{J}_P$ was plotted *vs.* $P^n_{(ex)}$, $P^n_{(in)}$ and *vs.* the term $(P_{(ex)}\cdot P_{(in)})^{n/2}$. As an example, the $1/\vec{J}_P$ *vs.* $(P_{(ex)}\cdot P_{(in)})^{n/2}$ plots are shown in Fig. 6. It was possible to construct linear plots by setting n equal to 2, whereas the usual Dixon plots were always curved. Although the experimental data were insufficient for a true fit, the above plots suggest that the self-inhibition of the phosphate flux follows the same pattern of concentration responsiveness as the increase of the flux at low phosphate concentrations.

Since the apparent self-inhibition constant, $K_{is(app)}$, could not be determined by fitting $1/\vec{J}_P$ *vs.* S^n, an alternative procedure was employed. If the ascending and the descending branches of the flux/-concentration curves follow the same pattern of concentration response, $K_{is(app)}$ can be estimated from the location of the flux-optimum, S_{opt}, by means of Eq. (9.2) (*cf.* methods section). Reading S_{opt} from the respective flux/concentration curves, $\vec{J}_P$ *vs.* $(P_{(ex)}\cdot P_{(in)})^{1/2}$, and inserting the graphically determined $K_{s(app)}$-values from Table 6, values of $K_{is(app)}$ in the range of 450–500 mM were found. The self-inhibition constants were almost independent of pH.

pH Dependence of the Unidirectional Phosphate Flux

Table 7 shows the equilibrium distribution of phosphate and chloride as well as the intracellular pH in amphotericin B treated cells and red cell ghosts. R_P, R_{Cl} and R_{P1} denote the equilibrium distributions of total phosphate, chloride and dihydrogen phosphate between intracellular and extracellular space. R_P and R_{Cl} were determined from the distribution of ^{32}P-phosphate, ^{36}Cl-chloride and D$(1-{}^3H)$glucose at

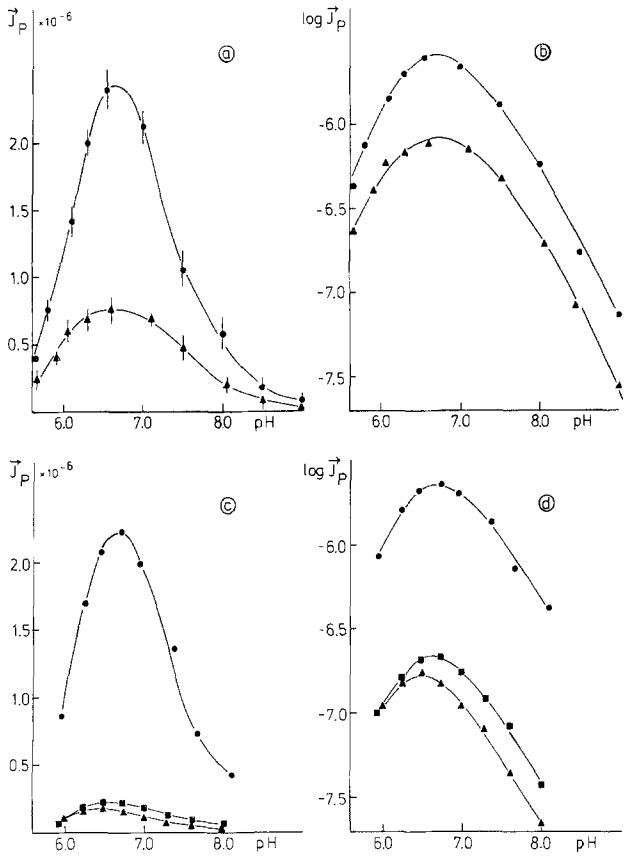

Fig. 7. pH dependence of the unidirectional phosphate flux in red cells (*a/b*) and in red cell ghosts (*c/d*). The unidirectional phosphate fluxes were determined from the tracer back-exchange at Donnan equilibrium. The experiments were executed at 25 °C with a 5% (wt/vol) cell suspension or with a red cell ghost suspension of an equivalent concentration. The red cells were pretreated with amphothericin B (5 μmol/liter) as described in the methods section. The red cell ghosts were prepared according to the methods of Bodemann and Passow [1] and Lepke and Passow [32]. Red cells: (*a*) flux/pH curves and (*b*) corresponding log-flux/pH curves. The closed circles (●) and the triangles (▲) indicate the mean value of three experiments, the vertical bars the standard deviation. Incubation solutions (in mM): (●) 130, K-phosphate; 30 sucrose; (▲) 40, K-phosphate; 30, sucrose. Sucrose was added in order to cancel out the osmotic pressure of hemoglobin. Red cell ghosts: (*c*) flux/pH curves and (*d*) log-flux/pH curves. The curves exhibit three single experiments. Incubation solutions (in mM): (●) 130, K-phosphate; 30, sucrose (=360 mosM); (■) 30, K-phosphate; 100, K_2SO_4; 30, sucrose (=355 mosM); (▲) 30, K-phosphate, 100, KCl, 50, sucrose (=325 mosM). The unidirectional phosphate fluxes, $\vec{J}_P$, were given in moles/(min · g cells)

isotopic equilibrium. The intracellular pH and R_{P1} were calculated from the chloride distribution and the extracellular pH as indicated in the methods section by using Eqs. (5) and (6). In amphotericin B treated red cells, $pH_{(in)}$ and $pH_{(ex)}$ are slightly different, but the differences are much smaller than in intact cells. As $pH_{(ex)}$ is increased, R_P is reduced. In the $pH_{(ex)}$-range of 5.5 to 8.0, R_{P1} equals R_{Cl}. Above a $pH_{(ex)}$ of 8.0, R_{P1} is smaller than R_{Cl}, suggesting that a Donnan distribution of phosphate has not been attained. In red cell ghosts, R_P and R_{Cl} are independent of pH, and $pH_{(in)}$ is nearly equal to $pH_{(ex)}$. Due to the addition of sucrose to the extracellular solution, R_P and R_{Cl} are slightly higher than unity.

Figure 7 displays the pH response of the unidirectional phosphate flux in amphotericin B (5 μmol/liter) treated red cells and in red cell ghosts. On the left, the fluxes are plotted *vs.* pH. On the right, the corresponding double logarithmic plots, $\log \vec{J}_P$ *vs.* pH, are shown. The flux/pH curves were measured at fixed phosphate concentrations, as indicated in the figure. The experiments with amphotericin B treated cells were conducted in phosphate solutions without maintaining isotonicity. In red cell ghosts, the phosphate concentrations were varied by iso-osmotic substitution of either chloride or sulfate for phosphate.

The unidirectional phosphate fluxes in amphotericin B treated red cells and in red cell ghosts exhibit the same pattern of pH response. The flux/pH curves are symmetric as can be seen best from the plots of $\log \vec{J}_P$ *vs.* pH. The pH optimum of the flux/pH curves is located at about pH 6.5, while the double logarithmic plots exhibit pH maxima at pH 6.7. The pH response is neither affected by variations of the phosphate concentration nor by the addition of chloride or sulfate. The curves of $\log \vec{J}_P$ *vs.* pH shift almost parallel as the phosphate concentration is changed.

The actual maximal phosphate flux, the pH-optimum, the pH values at $1/2 - \vec{J}_{max(opt/P)}$ at both sides of the pH maximum and the slopes, $\Delta \log \vec{J}_P / \Delta$ pH, for the upper and the lower branches of the flux/pH curves are listed in Table 8. The values were taken from the plots of $\log \vec{J}_P$ *vs.* pH as shown in Fig. 8. The pH optima taken from the double logarithmic plots were at about pH 6.7, while $pH_{(H/0.5)}$ and $pH_{(iH/0.5)}$ were at approximately 7.4 and 6.0, respectively. The upper branches of the curves from pH 7.3 to 9.0 and the lower branches from pH 6.3 to 5.6 can be fitted by straight lines. At a distance of approximately 1 pH unit away from the pH optimum, the slope of the upper branches is around −0.8 and that of the lower branches around +0.8, as far as the latter could be reliably determined. In ghosts, the pH range could not be extended to the same degree as in amphotericin B treated red cells. Therefore, on the lower branches of the flux/pH curves, at a pH below 6.3, only two to three points were available.

If the pK values of the activator and the inhibitor site differ in less than 2 pH units, then the

Table 8. pH optimum, flux optimum, pH-values at one-half maximal flux and slopes of the upper and the lower branches of the flux/pH curves[a]

Solution (mM)	pH values from the curves			$\vec{J}_{max(opt/P)}$	$\Delta \log \vec{J}_P/\Delta$ pH (pH < 6.3)	$\Delta \log \vec{J}_P/\Delta$ pH (pH > 7.3)
	$pH_{(H/0.5)}$	$pH_{(iH/0.5)}$	pH_{opt}			
Amphotericin B-treated red blood cells (25 °C)						
130, K-phosphate 30, sucrose	7.45	6.05	6.75	2.57×10^{-6}	0.84	−0.87
40, K-phosphate 30, sucrose	7.57	5.90	6.70	8.13×10^{-7}	0.83	−0.83
Red cell ghosts (25 °C)						
130, K-phosphate 30, sucrose	7.46	6.07	6.75	2.24×10^{-6}	(0.78)	−0.71
30, K-phosphate 100, K-sulfate 30, sucrose	7.38	6.00	6.70	2.24×10^{-7}	(0.78)	−0.70
30, K-phosphate 100, K-chloride 50, sucrose	7.22	(5.80)	6.50	1.74×10^{-7}	(0.46)	−0.75

[a] The values were determined from the plots of $\log \vec{J}_P$ *vs.* pH as shown in Fig. 8. The curves were fitted with a template by eye. $pH_{(H/0.5)}$ and $pH_{(iH/0.5)}$ are the pH-values at $1/2\text{-}\vec{J}_{max(opt/P)}$, pH_{opt} is the pH of the pH-optimum, and $\vec{J}_{max(opt/P)}$ the actual maximal flux of the flux/pH curves at constant phosphate concentration. The slopes, $\Delta \log \vec{J}_P/\Delta$ pH, were determined for the upper and the lower branches of the curves at a distance of approximately 1 pH unit apart from the pH optimum. For the slope of the upper branches the pH range of 7.3–9.0 was used; for the slope of the lower branches the pH range of 6.3–5.6 was employed as far as possible. The value $pH_{(iH/0.5)}$ in parenthesis was estimated by extrapolation because a sufficient number of points on the lower branch was not available.

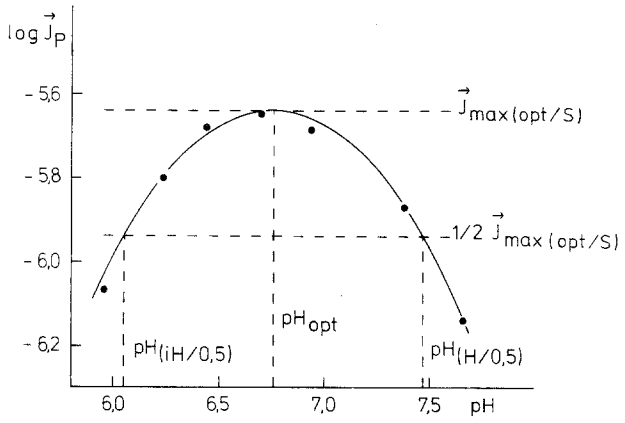

Fig. 8. Plotting procedure used for the determination of pH_{opt}, $pH_{(H/0.5)}$, and $pH_{(iH/0.5)}$. $pH_{(iH/0.5)}$ and $pH_{(H/0.5)}$, the pH at $1/2\text{-}\vec{J}_{max(opt/S)}$, were graphically determined from the intersection points of the curved lines and a horizontal line drawn at a distance of $0.3 = \log 0.5$ below the top of the curve $\log \vec{J}_P$ *vs.* pH. The points display the experimentally observed flux/pH curve for red cell ghosts at 130 mM K-phosphate as shown in Fig. 7d. The curved line was drawn with a template by fitting the points by eye. pH_{opt} can best be approximated by setting it equal to $0.5(pH_{(H/0.5)} + pH_{(iH/0.5)})$

respective pKs cannot be read directly from the flux/pH curves. In order to improve the analysis of the flux/pH curves, a series of replots was made, where the upper branches (pH > 6.5) and the lower branches (pH < 6.5) of the flux/pH curves were separately assessed. From the upper branches of the flux/pH curves, double reciprocal plots were made. The plots of $1/\vec{J}_P$ *vs.* $1/H_{(ex)}$ were linear. The slope of the straight lines decreases with increasing phosphate concentration, but the straight lines intersected the $1/H_{(ex)}$-axis at the same point (Fig. 9*a*). Correspondingly, linear plots were obtained for the upper branches of the flux/pH curves by plotting $\vec{J}_P$ *vs.* $\vec{J}_P/H_{(ex)}$ (not shown). Changes in the phosphate concentrations resulted in a parallel shift of the straight lines, but the slope of the straight lines was not affected. These features are indicative for a noncompetitive type of activation. Essentially similar results were obtained if the flux/pH curves were tested with reference to the intracellular pH.

As far as the lower branches of the flux/pH curves were concerned, the reciprocal phosphate flux was plotted *vs.* the extracellular proton concentration. In order to improve the accuracy of the plotting procedure, the $1/\vec{J}_P$-intercept from the corresponding double reciprocal plot made from the upper branch of the respective flux/pH curve was inserted as an additional point (Fig. 9*b*). The plots of $1/\vec{J}_P$ *vs.* $H_{(ex)}$ seem to be linear as well. The slope of the straight lines is reduced as the phosphate concentration is elevated, but the straight lines again intersect the $H_{(ex)}$-axis at approximately the same point. The plots of $1/\vec{J}_P$ *vs.* $H_{(ex)}$ point to a noncompetitive type of

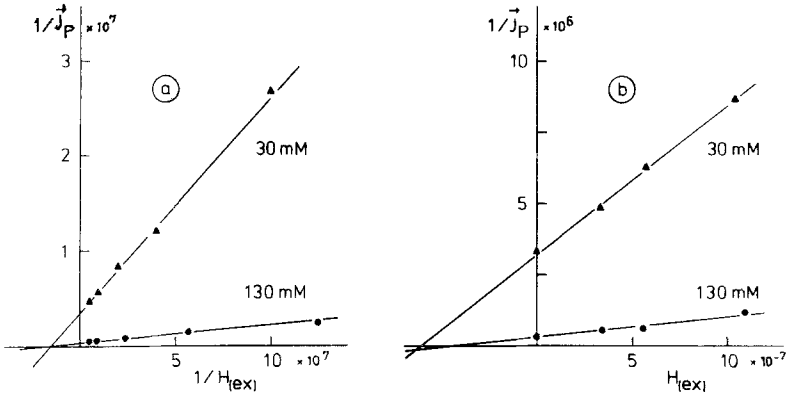

Fig. 9. Replots made from flux/pH curves. (*a*) Plots of $1/\vec{J}_P$ (moles/(min · g cells))$^{-1}$ *vs.* $1/H_{(ex)}$ (M)$^{-1}$ made from the upper branches (pH > 6.5) and (*b*) plots of $1/\vec{J}_P$ (moles/(min · g cells))$^{-1}$ *vs.* $H_{(ex)}$ (M) made from the lower branches (pH < 6.5) of the flux/pH curves. As an example, the flux/pH curves of red cell ghosts in K-phosphate/sucrose solution (130 mM K-phosphate, 30 mM sucrose) and in K-phosphate/K_2SO_4/sucrose solution (30 mM K-phosphate, 100 mM K_2SO_4, 30 mM sucrose) were used for the replots (*compare* Fig. 7c). The phosphate concentrations are indicated in the figure

Table 9. Apparent pK-values of the activator site, $pK_{(H/app)}$, and of the inhibitor site, $pK_{(iH/app)}$ as obtained from the flux/pH curves of phosphate[a]

Solution (mM)	Graphical determination			Calculated values	
	$pK_{(H/app)}$	$pK_{(iH/app)}$	$pK^*_{(iH/app)}$	$pK_{(H/app)}$	$pK_{(iH/app)}$
Amphotericin B-treated red blood cells (25 °C)					
130, K-phosphate 30, sucrose	7.35	6.40	6.15	7.01	6.49
40, K-phosphate 30, sucrose	7.48	6.15	6.02	7.26	6.24
Red cell ghosts (25 °C)					
130, K-phosphate 30, sucrose	7.20	6.36	6.15	7.01	6.49
30, K-phosphate 100, K-sulfate 30, sucrose	7.20	6.21	6.19	6.86	6.54
30, K-phosphate 100, K-chloride 50, sucrose	6.59	–	6.05	6.58	6.42

[a] The pK values were determined either by graphical analysis of the flux/pH curves or calculated from the pH optimum and the pH values at half-maximal flux by using Eqs. (10.5) and (10.6). *Compare* Table 8 and Fig. 8. $pK^*_{(iH/app)}$ was calculated from the pH optimum of the flux/pH curves by inserting $K_{(H/app)}$ into Eq. (10.5).

inhibition of the phosphate flux by protons at a low pH.

Alternatively, the pKs of the activator site and of the inhibitor site may be calculated from the pH optimum of the flux/pH curves. If the flux/pH curves are symmetric with respect to their pH response, the pH optimum and the pH-values at $1/2 - \vec{J}_{max(opt/S)}$ may be taken from the flux/pH curves as shown in Fig. 8. The pKs of the activator site and of the inhibitor site then can be calculated according to Eqs. (10.5) and (10.6) (*cf.* methods section). The apparent pKs are listed in Table 9. $pK_{(H/app)}$ is approximately 7.2, whereas the $pK_{(iH/app)}$ is about 6.1. The calculated apparent pK-values differ slightly from the graphically determined pK values.

Discussion

Phosphate Transport as Compared to the Transport of Sulfate and of Chloride

The kinetic mechanism of the anion transport across the red cell membrane is not known. Since other techniques have failed so far, we have to resort to kinetic studies in order to gain information concerning the transport mechanism. This paper deals with the kinetics of the phosphate transport across the erythrocyte membrane. As previous studies have shown, the phosphate transport across the red cell membrane is mediated by the same transport system as the transport of chloride and of sulfate. Argu-

ments in favor of this assumption come from kinetic studies as well as from biochemical studies. At first, a mutual competition of phosphate, chloride, and sulfate for the inorganic anion transport system was observed [10–12, 31, 55, 58, 70]. Secondly, the transport of phosphate, chloride and sulfate is inhibited by the same agents [3, 12–15, 19, 26, 29, 37, 39, 43, 53]. Finally, the most potent inhibitors of the anion transport DIDS (4,4′-diisothiocyanato-stilbene-2,2′-disulfonic acid) almost exclusively bind to a single membrane protein, the band-3 protein, which appears to play a pivotal role in anion transport across the red cell membrane [3–6, 8, 12, 13, 19, 28–30, 38–42, 44, 48, 49, 51, 52, 63, 70, 74, 77, 78]. On the other hand, the different anion species display considerable differences in their transport velocities and their pH response. Thus the question arises as to how a single transport system can account for these differences.

As shown in this paper, the unidirectional phosphate flux across the red cell membrane exhibits highly complex patterns of concentration response and of pH-responsiveness. At low phosphate concentrations, the unidirectional phosphate flux displays and *S*-shaped increase. The flux then passes a concentration maximum, and at high phosphate concentrations the flux decreases again. In contrast, the unidirectional fluxes of sulfate and of chloride display a simple saturation kinetics with a self-inhibition at high concentrations of the respective anions. The half-saturation concentrations of phosphate amount to approximately 65 mM (Tables 4 and 5) and are about 4 times higher than the half-saturation concentrations of sulfate under the same conditions. The half-saturation concentrations of chloride and of sulfate increase with increasing pH, while the half-saturation concentrations of phosphate seem to be independent of pH. At 25 °C, the unidirectional phosphate flux is approximately two times faster than the sulfate flux under the same conditions, while the chloride flux, if extrapolated to the same temperature, is 3–4 orders of magnitude faster than the phosphate flux. The pH response of the unidirectional fluxes of phosphate and of sulfate are almost identical, but the chloride fluxes display an entirely different pH response [2, 7, 9–13, 18, 25, 28, 41, 42, 53–60, 70, 73].

In contrast to sulfate and to chloride, phosphate can be incorporated into the organic phosphate pool of the red cells. Theoretically, the organic phosphate pool could act as an additional compartment which could modify the phosphate transport across the red cell membrane. However, the amounts of radioactive phosphate that, under our experimental conditions, were incorporated into the organic phosphate pool are negligible. Furthermore, the ^{32}P-phosphate back-exchange from radioactively labeled red cells follows a simple exponential function, pointing to a simple two-compartment system. Finally, recent studies with red cell ghosts have confirmed the *S*-shaped increase of the unidirectional phosphate flux, while the unidirectional sulfate flux did not show a pronounced sigmoidicity of the flux/concentration curves [60]. These observations indicate that the sigmoidal increase of the flux/concentration curves of phosphate reflects a property of the inorganic anion transport system rather than an alteration of the phosphate flux by the organic phosphate pool of the red blood cells.

The saturation of the unidirectional phosphate flux indicates that the phosphate anions on their way across the red cell membrane interact with a limited number of anion binding sites. For an *S*-shaped flux/concentration curve at least a two-site transport system has to be postulated. The anion binding sites which are directly involved in the anion transport across the red cell membrane were designated transport sites. The self-inhibition of the phosphate flux points to a second type of anion binding sites with a lower affinity for anions. These anion binding sites were termed modifier sites. Finally, the activity of the transport system appears to be regulated by two proton binding sites. The proton binding site with the higher pK was designated activator site, while the proton binding site with the lower pK was designated inactivator site.

The Interpretation of the Transport Equation

In general, the translocation of the anion across the cell membrane is assumed to be rate-determining, while at the membrane surfaces equilibria are established. The transport of an anion across the red cell membrane is analogous to an enzymatic reaction, where the breakdown of the substrate from the enzyme-substrate complex is rate-limiting for the overall reaction. For the analysis of the flux/concentration and of the flux/pH curves, therefore, plotting procedures can be employed that are commonly used in enzyme kinetics. These plotting procedures may serve as diagnostic tools in order to examine the precise pattern of concentration dependence and of pH dependence of the unidirectional fluxes.

In order to test the relative sigmoidicity of the flux/concentration curves, the Hill equation was adopted as a purely empirical equation in the same sense as it was introduced by Hill himself [27*a*]. Since the Hill equation can neither account for the pH dependence nor for the self-inhibition of the flux, two additional empirical terms were added. The

complete flux equation for the unidirectional phosphate flux then reads:

$$\vec{J}=\frac{\vec{J}_{max}}{(1+K_H/H+H/K_{iH})(1+K_s^n/S^n)(1+S^n/K_{is}^n)} \quad (9.0)$$

$\vec{J}_{max}$ – maximal theoretical flux
K_s, K_{is} – half-saturation constant, self-inhibition constant
n – Hill coefficient
K_H, K_{iH} – dissociation constants of the activator and of the inhibitor site
S, H – anion concentration, proton concentration.

At constant pH and at constant S the following abbreviations may be introduced:

$$\vec{J}_{max(pH)}=\vec{J}_{max}/(1+K_H/H+H/K_{iH}) \quad (11.1)$$

$$\vec{J}_{max(S)}=\vec{J}_{max}/(1+K_s^n/S^n)(1+S^n/K_{is}^n). \quad (11.2)$$

Substituting Eqs. (11.1) and (11.2) into Eq. (9.0) and rearranging yields Eqs. (9.1) and (10.1) as given in the methods section:

$$\vec{J}=\vec{J}_{max(pH)}\frac{S^n\cdot K_{is}^n}{(K_s^n+S^n)(K_{is}^n+S^n)} \quad (9.1)$$

$$\vec{J}=\vec{J}_{max(S)}/(1+K_H/H+H/K_{iH}). \quad (10.1)$$

$\vec{J}_{max(pH)}$ and $\vec{J}_{max(S)}$ are the maximal theoretical flux at constant pH and at constant S, respectively. A complete derivation of the transport equation would exceed the scope of the present paper. Therefore, as far as possible, references to textbooks of enzyme kinetics are given. Concerning the Hill equation, the reader is referred to Segel: Enzyme Kinetics pp. 360–380 [61]. As will be discussed below, Eqs. (9.0), (9.1), and (10.1) are based upon assumptions which are in accordance with our experimental results.

Equation (9.0) strictly applies to a diprotic transport system with a cooperative substrate binding. The term $(1+K_s^n/S^n)^{-1}$ provides a description for the binding of S to the transport sites and accounts for the sigmoidicity of the ascending branches of the flux/concentration curves. The term $(1+S^n/K_{is}^n)^{-1}$ describes the interaction of S with the modifier sites which are responsible for the self-inhibition at high S. The term $(1+K_H/H+H/K_{iH})^{-1}$ indicates the fraction of the transport systems which are in an active state. According to Eq. (9.0), the transport sites, the modifier sites, and the proton binding sites are capable of reacting independently of one another. Furthermore, the transport sites and the modifier sites are supposed to follow the same pattern of cooperativity.

There are several possibilities which may give rise to sigmoidal flux/concentration curves: (1) A cooperative binding of substrate to a multi-site transport system, where the transport rate is not affected by the binding of substrate to the transport sites. (2) The occupied transport sites of a multi-site transport system may interact to increase their transport rates. (3) Both the binding of substrate and the transport rates may be simultaneously affected. Irrespective of the precise mechanism of the cooperativity, the Hill equation assumes the transport to be dominated by the fraction of transport systems with the highest number of occupied transport sites. If this condition is not strictly met, then the Hill coefficient n no longer indicates the actual number of transport sites. Nevertheless, in many cases the experimental data can be fitted to the Hill equation by choosing a nonintegral value for n. As pointed out by Segel, the next integer above the experimentally determined apparent Hill coefficient is the minimum number of transport sites that are involved in the transport process.

As already outlined in the methods section, there are a number of plotting procedures for testing the concentration dependence of the flux/concentration curves. A serious obstacle to the graphical analysis arises from the fact that $\vec{J}_{max(pH)}$ cannot directly be obtained from the flux/concentration curves. Thus, the convenient plot of $\log(\vec{J}/(\vec{J}_{max(pH)}-\vec{J}))$ *vs.* $\log S$, where n is obtained from the slope of the plot, could not be used [Eq. (9.4.3)]. The apparent Hill coefficient n_{app} may be obtained from the initial slope of the double logarithmic plots [Eq. (9.4.1)], from the plots of $1/\vec{J}$ *vs.* $1/S^n$ [Eq. (9.5)] or from the plots of $\vec{J}$ *vs.* $\vec{J}/S^n$ [Eq. (9.6)]. The latter plotting procedures do not require $\vec{J}_{max(pH)}$ as a precondition but $J_{max(pH)}$ is obtained from the curve fitting procedures as a result (Table 1). It is not known whether the flux is regulated by the outer membrane surface, by the inner membrane surface, or whether both membrane surfaces participate in the regulation of the phosphate transport. The flux/concentration curves, therefore, were tested with reference to the extracellular phosphate concentration, $P_{(ex)}$, with reference to the intracellular phosphate concentration, $P_{(in)}$, and with reference to the term $(P_{(ex)}\cdot P_{(in)})^{1/2}$. This is tantamount to selecting either the extracellular solution, the intracellular solution, or the middle of the membrane as a reference state [27].

As indicated by Figs. 4 and 5, the ascending branches of the flux/concentration curves could be fitted to the Hill equation. The Hill plot parameters with reference to the term $(P_{(ex)}\cdot P_{(in)})^{n/2}$ were listed in Table 6. The apparent Hill coefficient n_{app} was always in the range of 1.6–1.8, indicating that at least two

substrate binding sites are involved in the transport of phosphate across the red cell membrane. Furthermore, $K_{s(app)}$ was almost independent of pH, while $\vec{J}_{max(pH/app)}$ exhibited a strong pH dependence. These results suggest that protons are not essential for the binding of phosphate to the transport system, but are required for the translocation of the phosphate anions across the membrane (*cf.*: Segel: System *A*1 and *A*2 pp. 888–907 [61]).

The self-inhibition was assumed to be completely noncompetitive and to follow the same sort of cooperativity as the increasing branches of the flux/-concentration curves. As mentioned already, the latter supposition for technical reasons could not be precisely tested. However, our experimental results supply some evidence to this assumption: (1) The usual Dixon plots were always curved, whereas the plots of $1/\vec{J}_P$ *vs.* $P_{(ex)} \cdot P_{(in)}$ were almost linear (Fig. 6). (2) The double logarithmic plots of $\log \vec{J}_P$ *vs.* $\log(P_{(ex)} \cdot P_{(in)})$ appeared to be symmetric. It should be stressed that in none of our flux/concentration curves the half-self-inhibition concentration could be reached. In view of these difficulties, the self-inhibition constant can best be estimated from the concentration optimum of the flux/concentration curves.

Finally, the term $(1+K_H/H+H/K_{iH})^{-1}$ accounts for the pH-response of the phosphate flux. The derivation of the term is based upon the following assumptions: (1) The inorganic anion transport system is supposed to function as a diprotic system which is activated by the binding of a first and inactivated by the binding of a second proton. (2) The binding of the protons is fast as compared to the binding of anions, and it is not affected by the anion concentration. (3) The transport system accepts HPO_4^{2-} and $H_2PO_4^-$ equally well. For details *see* Segel, Enzyme Kinetics, pp. 884–925 [61].

The flux/pH curves measured at fixed phosphate concentrations were bell-shaped (Fig. 7). They indicate that we have two sorts of proton binding sites, those with a higher pK that activate and others with a lower pK that inactivate the transport system. The plots of $1/\vec{J}_P$ *vs.* $1/H_{(ex)}$ for the upper branches and of $1/\vec{J}_P$ *vs.* $H_{(ex)}$ for the lower branches display a noncompetitive type of either activation or inhibition (Fig. 9). The noncompetitive activation of the phosphate transport indicates that the binding of protons to the activator site is not affected by the phosphate concentration and suggests that proton are not essential for the binding of phosphate to the transport sites. Otherwise, the intercepts on the $1/H_{(ex)}$-axis should change as the phosphate concentration is varied. Furthermore, the $1/\vec{J}_P$ *vs.* $1/H_{(ex)}$ plots were linear and did not show any indication for a sigmoidal concentration response with respect to the proton concentration. From these observations we concluded that the anion binding sites and the proton binding sites are independent of one another.

The symmetry of the flux/pH curves can be seen in particular from the $\log \vec{J}_P$ *vs.* pH plots (Figs. 7 and 8). Except for its sign, the upper and the lower branches of the curves have the same slope. If the transport system would either accept only the monovalent dihydrogen-phosphate or the divalent hydrogen-phosphate, then the flux/pH curves should display a strong asymmetry. Thus, the symmetry of the flux/pH curves provides strong evidence for the assumption that the transport system accepts $H_2PO_4^-$ and HPO_4^{2-} equally well.

The Accuracy of the Plotting Procedures

The physical meaning of the various parameters and the accuracy of the plotting procedures is difficult to assess. As pointed out already, the sigmoidicity of the flux/concentration curves and the K_s-values depend upon the actual number of transport sites and upon the strength of interaction between them. The Hill plots do not allow us to determine these two factors separately. The apparent Hill coefficients, therefore, indicate the minimum number of transport sites. Theoretically, if the cooperativity is weak, the number of transport sites may be higher than indicated by the apparent Hill coefficient. Since the apparent Hill coefficient enters exponentially into Eq. (9.1), it can be determined with high accuracy.

$K_{S(app)}$ and $K_{is(app)}$ are the apparent half-saturation and the apparent self-inhibition constant, and $\vec{J}_{max(pH/app)}$ is the maximal theoretical flux which would be observed if no self-inhibition would occur. As indicated in Table 1, $K_{s(app)}$, $K_{is(app)}$ and $\vec{J}_{max(pH/app)}$ are complex magnitudes. In general, the self-inhibition is perceived by deviations from linearity. However, as far as the self-inhibition is linear, it cannot be perceived from the plots. If the apparent Hill coefficient n is in the range of 1.6 to 1.8, then the true K_s and the true $\vec{J}_{max(pH)}$ are approximately 10% higher than $K_{s(app)}$ and $\vec{J}_{max(pH/app)}$, while the true K_{is} would be approximately 10% smaller than $K_{is(app)}$. These conclusions were further supported by computer simulations of the flux/concentration curves. As an example, the parameters obtained by graphical determination and by computer fit of a flux/concentration curve are tabulated in Table 10. It should be noted, that K_s and K_{is} are the half-saturation constant and the self-inhibition constant of the entire transport system which do not supply information about the intrinsic dissociation constants of the transport and the modifier

Table 10. Comparison between graphically determined parameters and computer-fit parameters[a]

Parameters		Graphical determination	Computer simulation
Flux/concentration curve, red cells, pH 7.2, 25 °C			
n	–	1.6 – 1.8	1.7 – 1.8
K_s	mM	79.5 ± 9.0	90 – 110
K_{is}	mM	375 ± 56	350 – 380
$\vec{J}_{max(S)}$	$\frac{\text{moles}}{\text{min} \cdot \text{g cells}}$	$(3.05 \pm 0.37) \times 10^{-6}$	$(3.5 - 3.9) \times 10^{-6}$
Flux/pH curve, red cell ghosts, 130 mM K-phosphate, 25 °C			
pK_H	–	7.20 (7.01)	7.0 – 7.1
pK_{iH}	–	6.15 (6.49)	6.4 – 6.5
$\vec{J}_{max(S)}$	$\frac{\text{moles}}{\text{min} \cdot \text{g cells}}$	$(2.9 - 3.1) \times 10^{-6}$	$(4.7 - 5.0) \times 10^{-6}$

[a] The flux/concentration curve measured at pH 7.2 (Fig. 1) and the flux/pH curve of red cell ghosts at 130 mM K-phosphate (Fig. 7c) were employed. Either the range or the mean ± standard deviation for the respective parameters are listed in the Table. The flux/concentration curves were analyzed with reference to the term $(P_{(ex)} \cdot P_{(in)})^{n/2}$. In red cell ghosts $pH_{(ex)} = pH_{(in)}$. The pK values calculated according to Eqs. (10.5) and (10.6) were placed between parentheses.

sites. The graphically determined apparent half-saturation constants, $K_{s(app)}$, and the graphically determined maximal fluxes $\vec{J}_{max(pH/app)}$, are always considerably higher than the half-saturation concentrations, $P_{(0.5)}$, and the actual fluxes $\vec{J}_{max(pH/opt)}$ as directly taken from the flux/concentration curves (Tables 4–6).

As mentioned already, the $pH_{(0.5)}$ values do not reflect the true pK values of the transport system (Tables 8 and 9). The true pK_H of the activator site should be lower than the graphically determined $pK_{(H/app)}$. Conversely, the true pK_{iH} of the inhibitor site should be higher than the apparent $pK_{(iH/app)}$. Although no systematic deviations were to be detected in the plots, the graphically determined values of $pK_{(H/app)}$ were about 0.3 pH units higher than those calculated according to Eqs. (10.5) and (10.6). Correspondingly, the graphically determined values of $pK_{(iH/app)}$ were approximately 0.3 pH units lower than the calculated ones (Table 9). The calculated pK_H and pK_{iH} values were consistent with the pKs obtained from the computer simulation of the respective flux/pH curves and seem to reflect the true pK values. On the contrary, the graphically determined values of $\vec{J}_{max(S)}$ were considerably lower than the values obtained from the computer simulations of the flux/pH curves. The reason for these discrepancies are unknown. With respect to the identification of ionizing groups, the differences between the graphically determined pKs and the computed pKs can be ignored.

Conclusions

According to our studies on the phosphate transport, the anion transport system of the red blood cell is constituted of two transport sites, two modifier sites, and two proton binding sites. The transport sites and the modifier sites are responsible for the *S*-shaped concentration dependence and for the self-inhibition of the phosphate flux, while the proton binding sites regulate the activity of the transport system. The binding characteristics of phosphate and the pH response of the phosphate flux suggest that the anion binding sites and the proton binding sites are separate sites which react independently of one another. The fact that the half-saturation constants were almost independent of pH while the maximal fluxes exhibited a pronounced pH response supplies strong evidence for the assumption that protons are not essential for the binding of phosphate to the transport sites but regulate the rate of translocation of phosphate across the red cell membrane. The sigmoidicity of the flux/concentration curves can be explained either by a two-site carrier or by an exchange transport mechanism. Since the flux measurements were performed at Donnan equilibrium, no information is gained about the position of the different sites at the membrane surfaces.

A part of these results was published at the 51th Meeting of the Deutsche Physiologische Gesellschaft at Kiel, 1979. This work was supported by the Deutsche Forschungsgemeinschaft.

References

1. Bodemann, H., Passow, H. 1972. Factors controlling the resealing of the membrane of human erythrocyte ghosts after hypotonic hemolysis. *J. Membrane Biol.* **8**:1–26
2. Brahm, J. 1977. Temperature-dependent changes of chloride transport kinetics in human red cells. *J. Gen. Physiol.* **70**:283–306
3. Cabantchik, Z.I., Knauf, P., Rothstein, A. 1978. The anion transport system of the red blood cell: The role of membrane protein evaluated by the use of "probes". *Biochim. Biophys. Acta* **515**:239–302
4. Cabantchik, Z.I., and Rothstein, A. 1974*a*. Membrane proteins related to anion permeability of human red blood cells. I. Localization of disulfonic stilbene binding sites in proteins involved in permeation. *J. Membrane Biol.* **15**:207–226
5. Cabantchik, Z.I., Rothstein, A. 1974*b*. Membrane proteins related to anion permeability of human red blood cells. II. Effects of proteolytic enzymes on disulfonic stilbene sites of surface proteins. *J. Membrane Biol.* **15**:227–248

6. Cabantchik, Z.I., Wolosin, J.M., Ginsburg, H., Zemel, O. 1977. Structural and functional properties of the anion transport system isolated from human erythrocyte membranes. *In:* Biochemistry of Membrane Transport. G. Semenza and E. Carafoli, editors. pp. 328–345. Springer-Verlag, Berlin – New York
7. Cass, A., Dalmark, M. 1973. Equilibrium dialysis of ions in nystatin-treated red cells. *Nature New Biol.* **244**:47–49
8. Cousin, J.L., Motais, R. 1979. Inhibition of anion permeability by amphiphilic compounds in human red cell: Evidence for an interaction of niflumic acid with the band 3 protein. *J. Membrane Biol.* **46**:125–153
9. Dalmark, M. 1975. Chloride transport in human red cells. *J. Physiol. (London)* **250**:39–64
10. Dalmark, M. 1976*a*. Effects of halides and bicarbonate on chloride transport in human red blood cells. *J. Gen. Physiol.* **67**:223–234
11. Dalmark, M. 1976*b*. Chloride in the human erythrocyte. Distribution and transport between cellular and extracellular fluids and structural features of the cell membrane. *Prog. Biophys. Mol. Biol.* **31**:145–164
12. Deuticke, B. 1970. Anion permeability of the red blood cell. *Naturwissenschaften* **57**:172–179
13. Deuticke, B. 1977. Properties and structural basis of simple diffusion pathways in the erythrocyte membrane. *Rev. Physiol. Biochem. Pharmacol.* **78**:1–97
14. Deuticke, B., Bentheim, M. von, Beyer, E., and Kamp, D. 1978. Reversible inhibition of anion exchange in human erythrocytes by an inorganic disulfonate, tetrathionate. *J. Membrane Biol.* **44**:135–158
15. Deuticke, B., Kim, M., Zöllner, C. 1973. The influence of amphotericin B on the permeability of mammalian erythrocytes to nonelectrolytes, anions and cations. *Biochim. Biophys. Acta* **318**:345–359
16. Drickamer, K. 1978. Orientation of the band 3 polypeptide from human erythrocyte membranes. Identification of NH_2-terminal sequence and site of carbohydrate attachment. *J. Biol. Chem.* **253**:7242–7248
17. Forster, R.E., Obaid, A.L., Crandall, E.D., Itada, N. 1980. Cl^- and HCO_3^- movements across the red cell membrane. *In:* Biophysics and Physiology of Carbon Dioxyde. C. Bauer, G. Gros, and H. Bartels, editors. p. 285. Springer-Verlag, Berlin – Heidelberg – New York
18. Funder, J., Wieth, J. 1976. Chloride transport in human erythrocytes and ghosts: A quantitative comparison. *J. Physiol. (London)* **262**:679–698
19. Gerhardt, S., Schöppe-Fredenburg, A., Schnell, K.F. 1973. Inhibition of sulfate transfer in human erythrocytes. *In:* Erythrocytes, Thrombocytes, Leukocytes. E. Gerlach, K. Moser, E. Deutsch, and W. Wilmans, editors. pp. 87–92. Thieme-Verlag, Stuttgart
20. Grinstein, S., Ship, S., Rothstein, A. 1978. Anion transport in relation to proteolytic dissection of band 3 protein. *Biochim. Biophys. Acta* **507**:294–304
21. Guidotti, G. 1977. The structure of intrinsic membrane proteins. *J. Supramol. Struct.* **7**:489–497
22. Gunn, R.B. 1972. A titratable carrier model for both mono- and di-valent anion transport in human red blood cells. *In:* Oxygen Affinity of Hemoglobin and Red Cell Acid-Base Status. M. Rorth and P. Astrup, editors. pp. 823–827. Munksgaard, Copenhagen
23. Gunn, R.B. 1978. Considerations of the titratable carrier model for sulfate transport in human red blood cells. *In:* Membrane Transport Processes. J.F. Hoffman, editor. pp. 61–77. Raven, New York
24. Gunn, R.B. 1979. Transport of anions across red Cell membranes. *In:* Membranes Transport in Biology. G. Giebisch, D. Tosteson, and H.H. Ussing, editors. Vol. 2, pp. 59–79. Springer-Verlag, Berlin – New York
25. Gunn, R., Dalmark, M., Tosteson, D., Wieth, J. 1973. Characteristics of chloride transport in human red blood cells. *J. Gen. Physiol.* **61**:185–206
26. Gunn, R.B., Fröhlich, O. 1979. Asymmetry in the mechanism for anion exchange in human red cell membranes: Evidence for reciprocating sites which react with one transported anion at a time. *J. Gen. Physiol.* **74**:351–374
27. Heinz, E. 1978. Mechanics and Energetics of Biological Transport. Springer-Verlag, Berlin – Heidelberg – New York
27*a*. Hill, A.V. 1910. A new mathematical treatment of changes of ionic concentration in muscle and nerve under the action of electric currents, with a theory as to their mode of excitation. *J. Physiol. (London)* **40**:190–224
28. Knauf, P.A. 1979. Erythrocyte anion exchange and the band 3 protein: Transport kinetics and molecular structure. *In:* Current Topics in Membrane and Transport. Vol. 90, pp. 249–363. Academic Press, New York – San Francisco – London
29. Ku, C.P., Jennings, M.L., Passow, H. 1979. A comparison of the inhibitory potency of reversibly acting inhibitors of anion transport on chloride and sulfate movements across the human red cell membrane. *Biochim. Biophys. Acta* **553**:132–141
30. Lepke S., Fasold, H., Pring, M., Passow, H. 1976. A study of the relationship between inhibition of anion exchange and binding to the red blood cell membrane of 4,4′-diisothiocyano stilbene-2,2′ disulfonic acid (DIDS) and of its dihydro derivative (H_2DIDS). *J. Membrane Biol.* **29**:147–177
31. Lepke, S., Passow, H. 1971. The permeability of the human red blood cell to sulfate ions. *J. Membrane Biol.* **6**:158–182
32. Lepke, S., Passow, H. 1972. The effect of pH at hemolysis on the reconstitution of low cation permeability in human erythrocyte ghosts. *Biochim, Biophys. Acta* **255**:696–702
33. Motais, R., Cousin, J.L. 1976. Inhibitory effect of ethacrynic acid on chloride permeability. *Am. J. Physiol.* **231**:1485–1489
34. Motais, R., Cousin, J.L. 1978. A structure activity study of some drugs acting as reversible inhibitors of chloride permeability in red cell membranes: Influence of ring substituents. *In:* Cell Membrane Receptors for Drugs and Hormones: A Multidisciplinary Approach. R.W. Straub and L. Blis, editors. pp. 219–225. Raven, New York
35. Motais, R., Sola, F., Cousin, J.L. 1978. Uncouplers of oxidative phosphorylation. A structure-activity study of their inhibitory effect on passive chloride permeability. *Biochim. Biophys. Acta* **510**:201–207
36. Obaid, A.L., Crandall, E.D., Forster, R.E. 1978. $HCO_3^- - Cl^-$ exchange in human erythrocytes: Effects of pH and temperature. *Fed. Proc.* **37**:313
37. Obaid, A.L., Rega, A.F., Garrahan, P.J. 1972. The effects of maleic anhydride on the ionic permeability of red cells. *J. Membrane Biol.* **9**:385–401
38. Passow, H. 1977. Anion transport across the red blood cell membrane and the protein in band 3. *Acta Biol. Med. Ger.* **36**:817–821
39. Passow, H. 1978. The binding of 1-fluoro-2,4-dinitrobenzene and of certain stilbene-2,2′-disulfonic acids to anion permeability-controlling sites on the protein in band 3 of the red blood cell membrane. *In:* Cell Membrane Receptors for Drugs and Hormones: A Multidisciplinary Approach. R.W. Straub and L. Bolis, editors. pp. 203–218. Raven, New York
40. Passow, H., Fasold, H., Lepke, S., Pring, M., Schuhmann, B. 1977b. Chemical and enzymic modification of membrane proteins and anion transport in human red blood cells. *In:* Membrane Toxicity. M.W. Miller and A.E. Shamoo, editors. pp. 353–377. Plenum, New York
41. Passow, H., Fasold, H., Zaki, L., Schuhmann, B., Lepke, S. 1975. Membrane proteins and anion exchange in human eryth-

rocytes. *In:* Biomembranes: Structure and Function. G. Gardos and I. Szasz, editors. pp. 197–214. North-Holland, Amsterdam
42. Passow, H., Pring, M., Legrum-Schuhmann, B., Zaki, L. 1977a. The action of 2-(4′-aminophenyl)-6-methyl benzene thiazol-3,7′-disulfonic acid (APMB) on anion transport and the protein in band 3 of the red blood cell membrane. *In:* Biochemistry of Membrane Transport. G. Semenza and E. Carafoli, editors. pp. 306–315. Springer-Verlag, Berlin – New York
43. Passow, H., Schnell, K.F. 1969. Chemical modifiers of passive ion permeability of the erythrocyte membrane. *Experientia* **25**:460–468
44. Passow, H., Zaki, L. 1978. Studies on the molecular mechanism of anion transport across the red blood cell membrane. *In:* Molecular Specialization and Symmetry in Membrane Function. A.K. Solomon and M. Karnovsky, editors. pp. 229–250. Harvard University Press, Cambridge
45. Reichstein, E., Blostein, R. 1975. Arrangement of human erythrocyte membrane proteins. *J. Biol. Chem.* **25**:6256–6263
46. Ross, A.H., McConnell, H.M. 1977. Reconstitution of band 3, the erythrocyte anion exchange protein. *Biochem. Biophys. Res. Commun.* **74**:1318–1325
47. Ross, A.H., McConnell, H.M. 1978. Reconstitution of the erythrocyte anion channel. *J. Biol. Chem.* **253**:4777–4782
48. Rothstein, A. 1978. The functional roles of band 3 protein of the red blood cell. *In:* Molecular Specialization and Symmetry in Membrane Function. A.K. Solomon and M. Karnovsky, editors. pp. 128–159. Harvard University Press, Cambridge
49. Rothstein, A., Cabantchik, Z.I. 1974. Protein structures involved in the anion permeability of the red blood cell membrane. *In:* Comparative Biochemistry and Physiology of Transport. L. Bolis, K. Bloch, S.E. Luria, and F. Lynen, editors. pp. 354–362. North-Holland, Amsterdam
50. Rothstein, A., Cabantchik, Z.I., Balshin, M., Juliano, R. 1975. Enhancement of anion permeability in lecithin vesicles by hydrophobic proteins extracted from red blood cell membranes. *Biochim. Biophys. Res. Commun.* **64**:144–150
51. Rothstein, A., Cabantchik, Z., Knauf, P. 1976. Mechanism of anion transport in red blood cells: Role of membrane proteins. *Fed. Proc.* **35**:3–10
52. Rothstein, A., Grinstein, S., Ship, A., Knauf, P.A. 1978. Asymmetry of functional sites of the erythrocyte anion transport protein. *Trends Biochem. Sci.* **3**:126–128
53. Schnell, K.F. 1972. On the mechanism of inhibition of the sulfate transfer across the human erythrocyte membrane. *Biochim. Biophys. Acta* **282**:265–276
54. Schnell, K.F. 1977. Anion transport across the red blood cell membrane mediated by dielectric pores. *J. Membrane Biol.* **37**:99–136
55. Schnell, K.F. 1979. The anion transport system of the red blood cell. *In:* Biophysics of Membrane transport. Vth Winter School on Biophysics of Membrane Transport School Proceedings, Vol. II. pp. 216–252, Wrocław, Poland
56. Schnell, K.F., Besl, E., Kolb, G. 1980. The concentration response of the unidirectional sulfate and phosphate flux in red cell ghosts. *Pfluegers Arch.* **384**:R13
57. Schnell, K.F., Gerhardt, S. 1973. The effect of membrane potential on the anion exchange across the erythrocyte membrane. *Pfluegers Arch.* **343**:R60
58. Schnell, K.F., Gerhardt, S., Schöppe-Fredenburg, A. 1977. Kinetic characteristics of the sulfate self-exchange in human red blood cells and red blood cell ghosts. *J. Membrane Biol.* **30**:319–350
59. Schnell, K.F., Mosel, R. von der. 1979. Studies on the phosphate transport across the red blood cell membrane: The concentration dependence of the unidirectional phosphate flux. *Pfluegers Arch.* **379**:R25
60. Schnell, K.F., Mosel, R. von der. 1979. Studies on the phosphate transport across the red blood cell membrane: The analysis of the flux/concentration curves. *Pfluegers Arch.* **379**:R27
61. Segel, I.H. 1975. Enzyme Kinetics, Behavior and Analysis of Rapid Equilibrium and Steady-State Enzyme Systems. John Wiley & Sons, New York – London – Sidney – Toronto
62. Shami, Y., Carver, J., Ship, S., Rothstein, A. 1977. Inhibition of Cl^- binding to anion transport protein of the red blood cell by DIDS (4,4′-diisothiocyano-2,2′-stilbene disulfonic acid) measured by (^{36}Cl) NMR. *Biochem. Biophys. Res. Commun.* **76**:429–436
63. Shami, Y., Rothstein, A., Knauf, P.A. 1978. Identification of the Cl^- transport site. *Biochim. Biophys. Acta* **508**:357–363
64. Steck, T.L. 1974. The organization of proteins in the human red blood cell membrane. *J. Cell Biol.* **62**:1–19
65. Steck, T.L. 1978. The band 3 protein of the human red cell membrane: A review. *J. Supramol. Struct.* **8**:311–324
66. Steck, T.L., Koziarz, J.J., Singh, M.K., Reddy, R., Kohler, H. 1978. Preparation and analysis of seven major, topographically defined fragments of band 3, the predominant transmembrane polypeptide of human erythrocyte membranes. *Biochemistry* **17**:1216–1222
67. Steck, T.L., Ramos, B., Strapazon, E. 1976. Proteolytic dissection of band 3, the predominant transmembrane polypeptide of the human erythrocyte membrane. *Biochemistry* **15**:1154–1161
68. Tanner, M.J.A. 1978. Erythrocyte glycoproteins. *Curr. Top. Membr. Transp.* **11**:279–325
69. Tanner, M.J.A. 1979. Isolation of integral membrane proteins and criteria for identifying carrier proteins. *Curr. Top. Membr. Transp.* **12**:1–51
70. Vangala, R., Schnell, K.F. 1979. Studies on the phosphate transport across the red blood cell membrane: The inhibition of the unidirectional phosphate flux by chloride and sulfate. *Pfluegers Arch.* **379**:R25
71. Weast, R.C. 1976. Handbook of Chemistry and Physics. (56th Ed.) CRC-Press, Cleveland
72. Webb, J.L. 1963. Enzyme and metabolic inhibitors. Academic Press, New York – London
73. Wieth, J.O., Dalmark, M., Gunn, R.B., Tosteson, D.C. 1973. The transfer of monovalent inorganic anions through the red cell membrane. *In:* Erythrocytes, Thrombocytes, Leukocytes. E. Gerlach, K. Moser, E. Deutsch, and W. Wilmanns, editors. pp. 71–76. Thieme-Verlag, Stuttgart
74. Wolosin, J.M., Ginsburg, H., Cabantchik, Z.I. 1977. Functional characterization of anion transport system isolated from human erythrocyte membranes. *J. Biol. Chem.* **252**:2419–2427
75. Yu, J., Steck, T.L. 1975a. Isolation and characterization of band 3, the predominant polypeptide of the human erythrocyte membrane. *J. Biol. Chem.* **250**:9170–9175
76. Yu, J., Steck, T.L. 1975b. Associations of band 3, the predominant polypeptide of the human erythrocyte membrane. *J. Biol. Chem.* **250**:9176–9184
77. Zaki, L., Fasold, H., Schuhmann, B., Passow H. 1975. Chemical modification of membrane proteins in relation of inhibition of anion exchange in human red blood cells. *J. Cell. Physiol.* **86**:471–494
78. Zaki, L., Ruffing, W., Gartner, E.M., Fasold, H., Motais, R., Passow, H. 1977. Band 3 as site of action of reversibly binding inhibitors of anion transport across the red cell membrane. *FEBS Meet.*, Copenhagen, *Abstr.* A4-17-671

Received 24 July 1980; revised 9 January 1981